CISS02

THREE-BODY SCATTERING THEORY AND ITS APPLICATIONS

Yasuro Koike
Hosei U. and CNS

Three-Body Scattering Theory and Its Applications

I. An Introduction to Three-Body Scattering Theory (Faddeev Theory)

II. An Introduction to the Three-Nucleon Studies

III. Application to Light Nuclear Systems — Three-Body Resonances

QUANTUM MECHANICAL SOLUTION FOR A GIVEN HAMILTONIAN

APPROACH I

Schrödinger eqn(Differential equation)
+ Boundary condition

APPROACH II

Integral equation
Boundary condition included in the equation

Two different approach to obtain the SAME solution

APPROACH I

Boundary condition (two-body case)

- bound states

  $\Psi(\vec{r}) = 0$ as $r \to \infty$.
- scattering states

  $\Psi(\vec{r}) =$

  (incident plane wave)

  $+$ (outgoing spherical wave)

  as $r \to \infty$.

Boundary condition (three-body case)

- bound states

  $\Psi(\vec{x}, \vec{y}) = 0$ as $x, y \to \infty$.
- scattering states

  No description in TEXTBOOKS !!

TWO-BODY SCATTERING THEORY IN THE MOMENTUM SPACE

Hamiltonian

For V with finite range:

$$H = H_0 + V \tag{1}$$

Lippmann-Schwinger equation

$$|\Psi(E)> = |\vec{p}> + G_0(E)V|\Psi(E)> . \tag{2}$$

The first term is one of the boundary condition: incident plane wave.
The second term should go to outgoing spherical wave at infinity.

The Green's function

$$G_0(E) = (E - H_0)^{-1} \tag{3}$$

Note: Operating $(E - H_0)$ on eq.(2), you get Schrödinger equation back.

$(E - H_0)G_0(E) = 1, (E - H_0)|p> = 0.$

Evaluation of operators in momentum space

$$< \vec{p}|H|\vec{p'} >= \delta^3(\vec{p}-\vec{p'})\ p^2/2\mu + < \vec{p}|V|\vec{p'} > \quad (4)$$

$$< \vec{p}|G_0(E)|\vec{p'} >= \frac{\delta^3(\vec{p}-\vec{p'})}{E - p^2/2\mu} \quad (5)$$

- $G_0(E)$ is singular for $E > 0$ at on-shell p: *i.e.*, $p^2/2\mu = E$.

Boundary condition

$$E : E + i\epsilon\ ,\ \epsilon \to 0 \quad (6)$$

makes the second term of L-S equation to be outgoing spherical wave.

- regular for $E < 0$.

Bound state:

No singularity in $G_0 \Rightarrow$ No outgoing wave

No incident wave

L-S equation for the bound state

$$|\Psi(E)> = G_0(E)V|\Psi(E)> . \tag{7}$$

HOW DO YOU SOLVE TWO-BODY EQUATIONS?

Basic equation for bound states:

$$|\Psi(E)> = G_0(E)V|\Psi(E)>, \; E < 0. \qquad (1)$$

Basic equation for scattering states:

$$|\Psi(E)> = |\vec{p}> + G_0(E)V|\Psi(E)>, \; E > 0. \qquad (2)$$

Note that boundary conditions are included in the equation through the analyticity.

SIMPLIFY THE EQUATION

Angular momentum decomposition

+ Fourier transform for V

$\Rightarrow V_\ell(p, p')$

METHOD FOR BOUND STATES

To make the bound state equation to a standard equation, we introduce $\eta(E)$ where

$$\eta(E)|\Psi(E)>= G_0(E)V|\Psi(E)> \qquad (3)$$

Or

$$\eta(E)\Psi_\ell(p,E) = \int_0^\infty p'^2 dp' \frac{V_\ell(p,p')\Psi_\ell(p',E)}{E - p'^2/2\mu} \qquad (4)$$

$\eta(E)$ is the eigenvalue of $G_0(E)V$, which is a real number at $E < 0$. Replacing the integral by numerical sum, you have a matrix eigenvalue problem which can be solved numerically.

For given E, you solve the eigenvalue equation. Changing E, you eventually find an energy E with $\eta(E) = 1$.

NOTE

A potential $V/\eta(E)$ would have a bound state at E.

METHOD FOR SCATTERING STATES

Note that full wave functions are not much interesting in the scattering problems.

L-S equation for T-operator

$$T(E) = V + VG_0(E)T(E) \tag{5}$$

with

$$T(E)|\vec{p}> \equiv V|\Psi(E;\vec{p})> \tag{6}$$

T-matrix

$$T(E;\vec{p},\vec{p'}) = <\vec{p}|T(E)|\vec{p'}> \tag{7}$$

After angular momentum decomposition

$$T(E;p,p') = V(p,p') + \int_0^\infty k^2 dk \frac{V(p,k)T(E;k,p')}{E - k^2/2\mu} \tag{8}$$

Replacing the integral by numerical sum, you have linear algebraic equations which can be solved numerically.

A special care should be taken to the singularity.

$$\int_0^\infty \frac{dk}{p+i\epsilon-k} \Rightarrow P\int_0^\infty \frac{dk}{p-k} - i\pi\delta(p-k) \qquad (9)$$

Some important remarks on $T(E;,p,p')$

T-matrix is called on-the-energy-shell(on-shell) if $E=p^2/(2\mu)=p'^2/(2\mu)$.

We generalize it to off-shell where E,p,p' are independent. Off-shell t-matrix is the input to 3-bod eqs.

T-matrix is real at $E<0$, and complex at $E>0$.

T is singular at the two-body binding energy.

In the vicinity of the binding energy, T is well described by

$$T(E;p,p') = \frac{<p|V|\Psi><\Psi|V|p'>}{E-\epsilon_0} \qquad (10)$$

with ϵ_0 the binding energy and $\Psi(p)$ the bound state wave function.

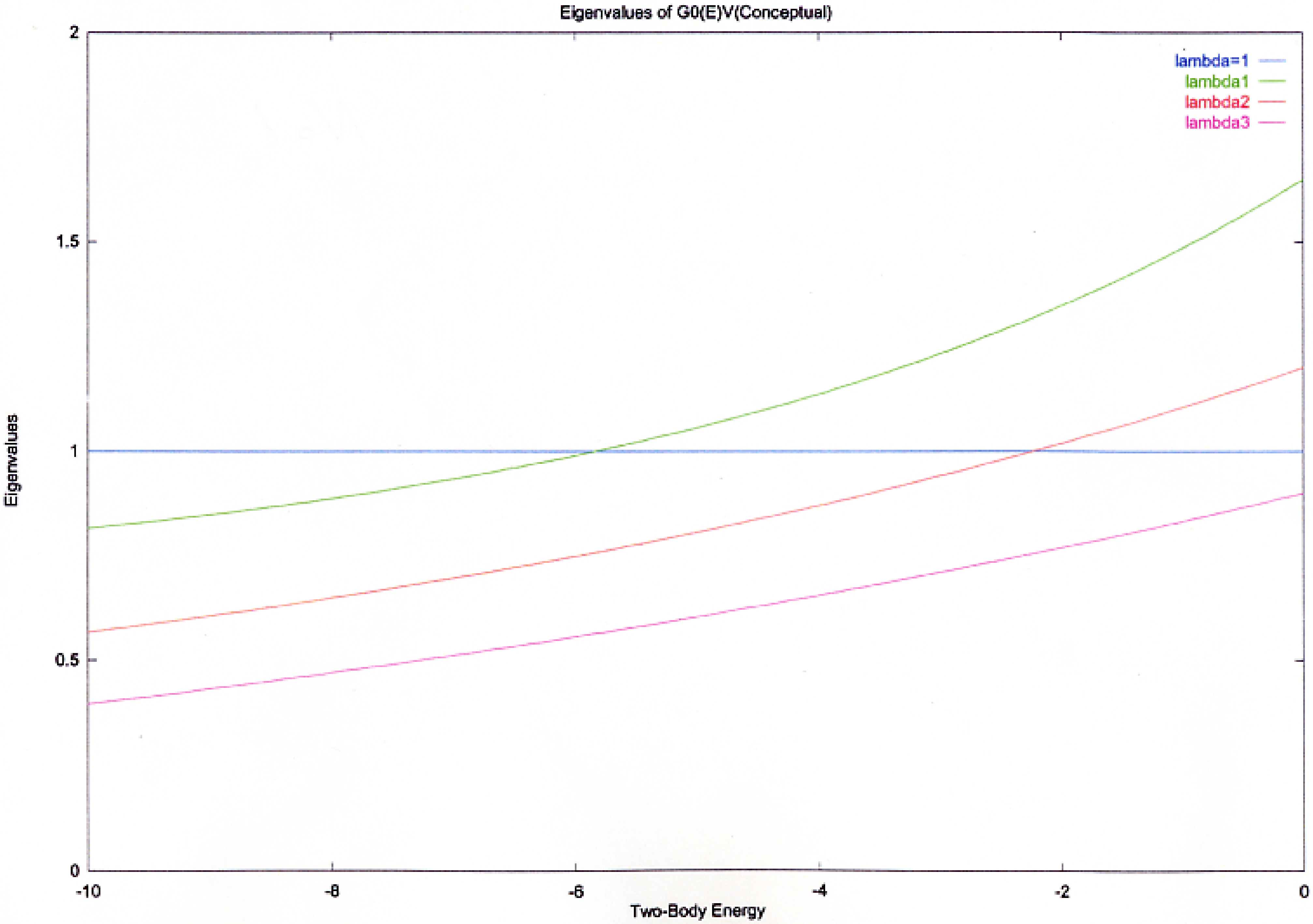

Eigenvalues of G0(E)V(Conceptual)
lambda=1
lambda1
lambda2
lambda3
Eigenvalues
Two-Body Energy
2
1.5
1
0.5
0
-10
-8
-6
-4
-2
0

Hamiltonian

For V_α with finite range:

$$H = H_0 + \sum_{\alpha=1}^{3} V_\alpha \tag{1}$$

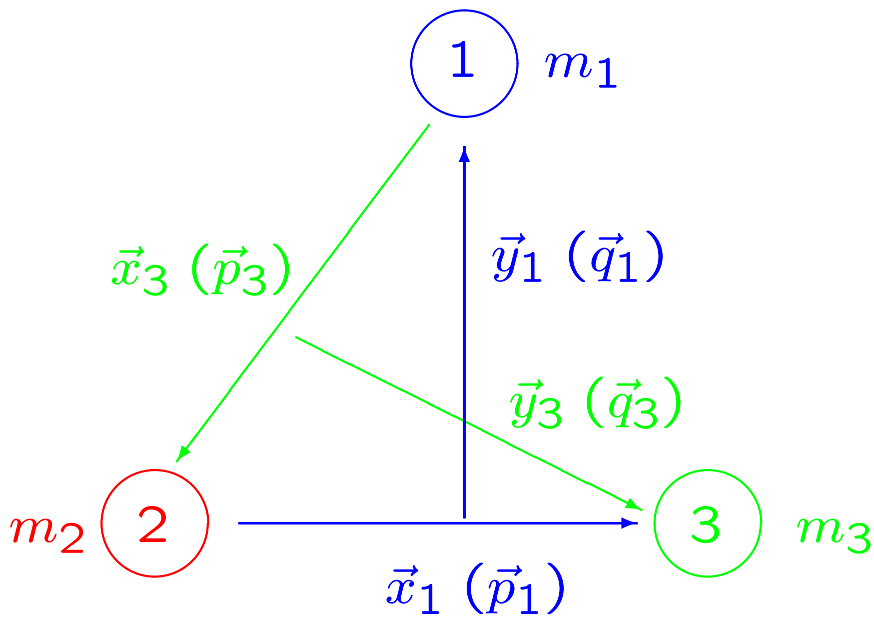

particle 1: the spectator under V_1

particle 2: the spectator under V_2

particle 3: the spectator under V_3

x_α, y_α: Jacobi coordinate

p_α: the momentum corresponding to x_α

q_α: the momentum corresponding to y_α

THREE-BODY SCATTERING EQUATIONS

A.G.S. eqs., one of the variations of Faddeev eqs.

AGS eqs.

$$
\begin{aligned}
U_{\alpha\beta}(E) &= (E - H_0)(1-\delta_{\alpha\beta}) \\
&\quad + \sum_{\gamma\neq\alpha} T_\gamma(E) G_0(E) U_{\gamma\beta}(E),
\end{aligned}
\tag{2}
$$

with

$$
T_\gamma(E) = V_\gamma + V_\gamma G_0(E) T_\gamma(E). \tag{3}
$$

$T_\gamma(E)$ and $G_0(E)$ contain all dynamical information including boundary conditions.
In order to understand the structure of the three-body equations, we iterate eqs. (3)

$$
\begin{aligned}
U_{\alpha\beta}(E) &= (E - H_0)(1-\delta_{\alpha\beta}) \\
&+ \sum_{\gamma\neq\alpha,\gamma\neq\beta} T_\gamma(E) \\
&+ \sum_{\gamma\neq\alpha,\delta\neq\gamma} T_\gamma(E) G_0(E) T_\delta(E) G_0(E) U_{\delta\beta}(E)
\end{aligned}
\tag{4}
$$

Namely, successive T-matrix should be different.

SCATTERING BOUNDARY CONDITIONS

Two-Body

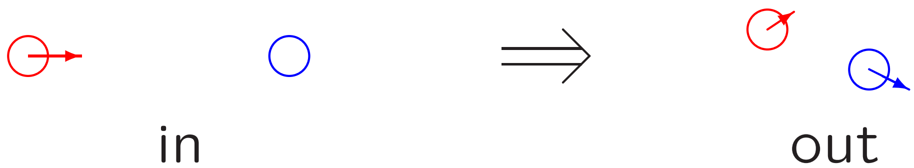

Three-Body

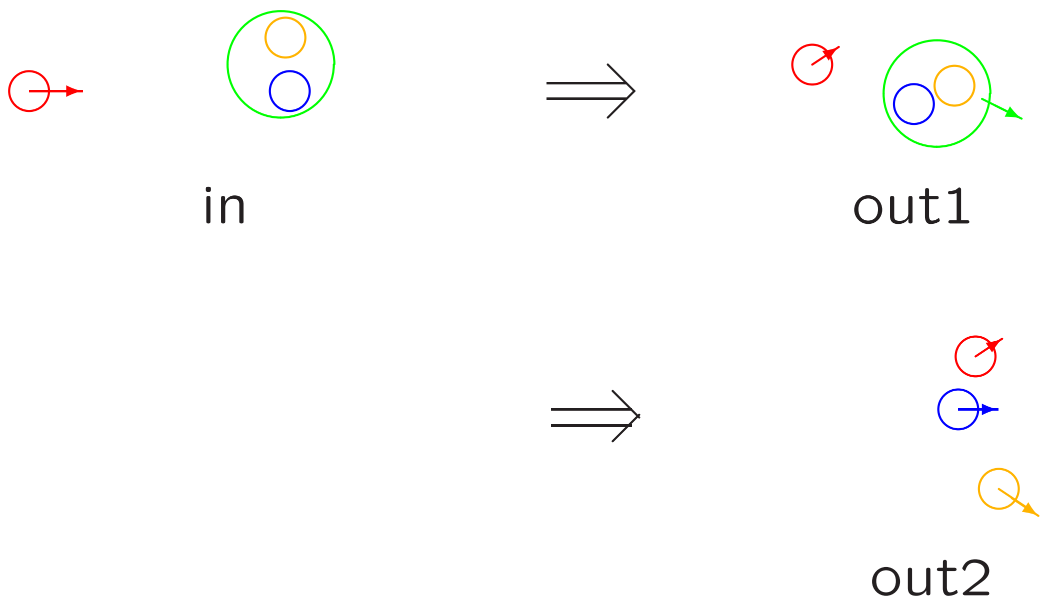

Out1(elastic), out2(breakup),
and even out3(rearrangement) should
simultaneously be described.

The Green's function

$$G_0(E) = (E - H_0)^{-1} \tag{5}$$

in the momentum representation

$$G_0(E) = \frac{1}{E - p_1^2/2\mu_{2-3} - q_1^2/2\mu_{1-(2,3)}} \tag{6}$$

with

$$\frac{1}{\mu_{2-3}} = \frac{1}{m_2} + \frac{1}{m_3} \tag{7}$$

$$\frac{1}{\mu_{1-(2,3)}} = \frac{1}{m_1} + \frac{1}{m_2 + m_3}. \tag{8}$$

Note that $G_0(E)$ is singular not at a fixed momentum, but in a certain range.

This is the breakup boundary condition.

Two-Body T-matrix $T_\gamma(E)$

Two-Body energy is evaluated by
(Total energy) - ($K.E.$ of the spectator)

$$E - q_\gamma^2/2\mu_{\gamma-(\alpha,\beta)}$$

$T_\gamma(E)$ is singular when the two-body energy is the binding energy of the two-body system

$$\Downarrow$$

Boundary condition corresponding to 2-cluster scattering channel:
particle-γ + binding pair(α, β).

EXAMPLE: THE NEUTRON-NEUTRON-PROTON SYSTEM

Let the proton be particle no.3.
T_1 and T_2 are singular because of the deuteron.
Most singular part is, therefore, $T_1 G_0 T_2$.
This operator is evaluated by
$< \vec{q}_1 \vec{p}_1|, \ |\vec{q}_2 \vec{p}_2 >$.

In the vicinity of the binding energy,

$$T_1 = |g_1 > \tau_1(E) < g_1| \tag{9}$$

where $\tau_1(E)$ has a pole at the binding energy. Defining $Z_{12}(E)$ by

$$Z_{12}(E) \equiv < g_1|G_0(E)|g_2 > \tag{10}$$

we derive one-dimensional integral equations with $\vec{q}_\alpha$, the spectator momentum. The resulting equations are two-body like integral equations with complex $Z(E)$ which behave like a complex potential, and with $\tau(E)$ which behave like the Green's function in the two-body equation.

$$X_{\alpha\beta}(E) = Z_{\alpha\beta}(E) + \sum Z_{\alpha\gamma}(E)\tau_\gamma(E)X_{\gamma\beta}(E) \tag{11}$$

which should be compared with

$$T(E) = V + VG_0(E)T(E) \tag{12}$$

Let us observe an example of the singularities in $Z_{12}(E)\tau_2(E)$ numerically.

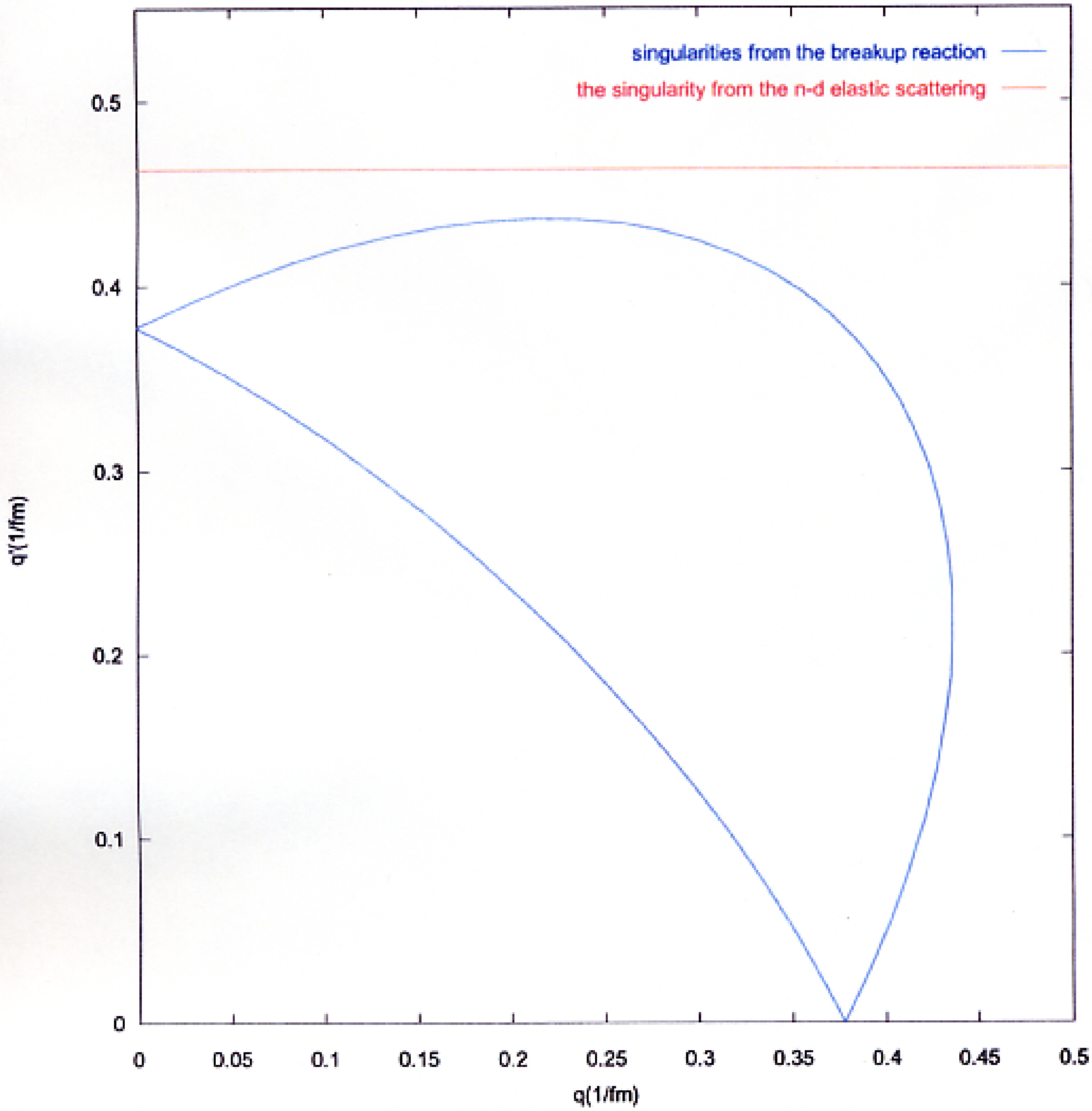

singularities from the breakup reaction
the singularity from the n-d elastic scattering
q'(1/fm)
q(1/fm)
0
0.1
0.2
0.3
0.4
0.5
0
0.05
0.1
0.15
0.2
0.25
0.3
0.35
0.4
0.45
0.5

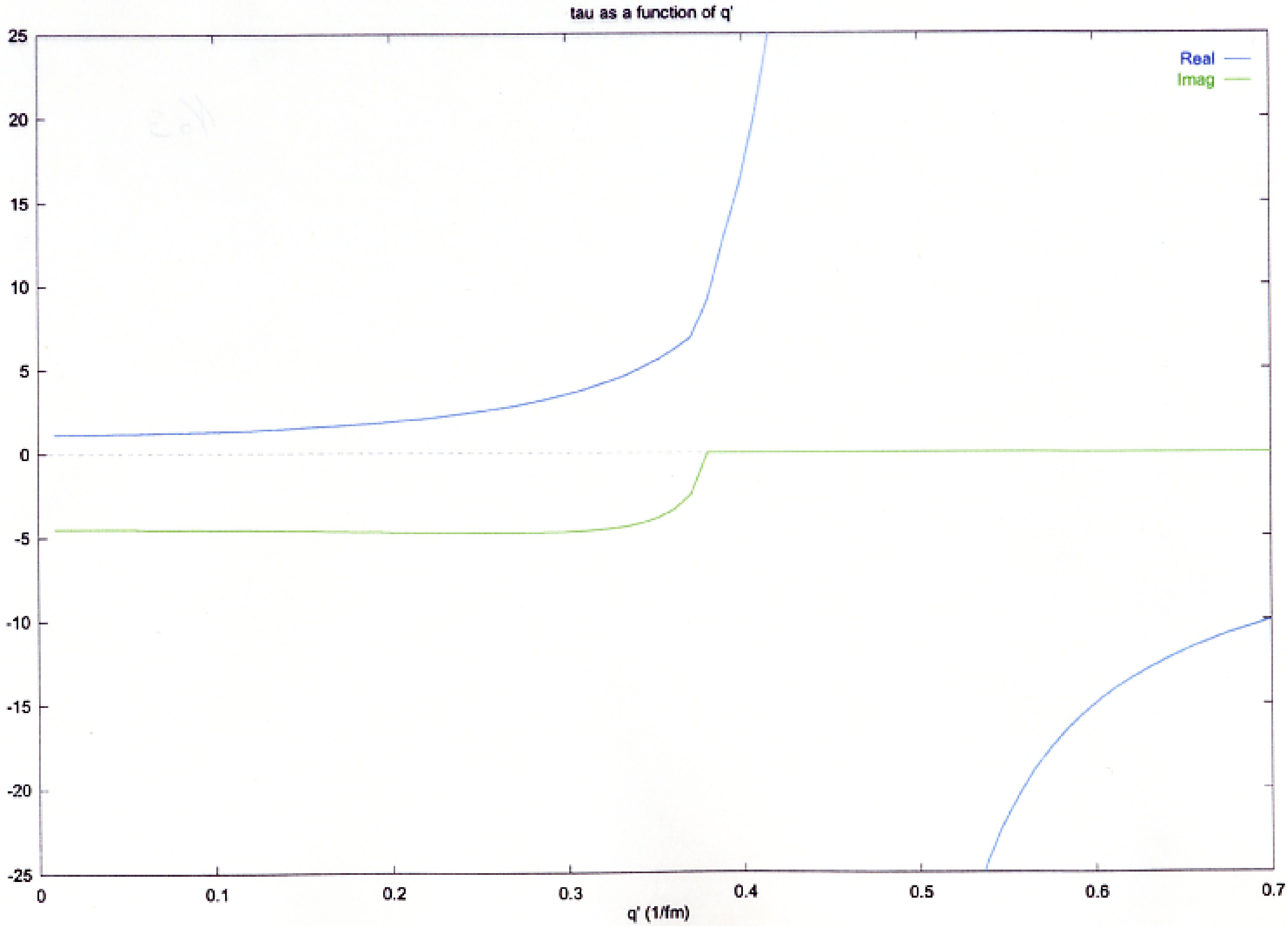

tau as a function of q'
Real
Imag
25
20
15
10
5
0
-5
-10
-15
-20
-25
0
0.1
0.2
0.3
0.4
0.5
0.6
0.7
q' (1/fm)

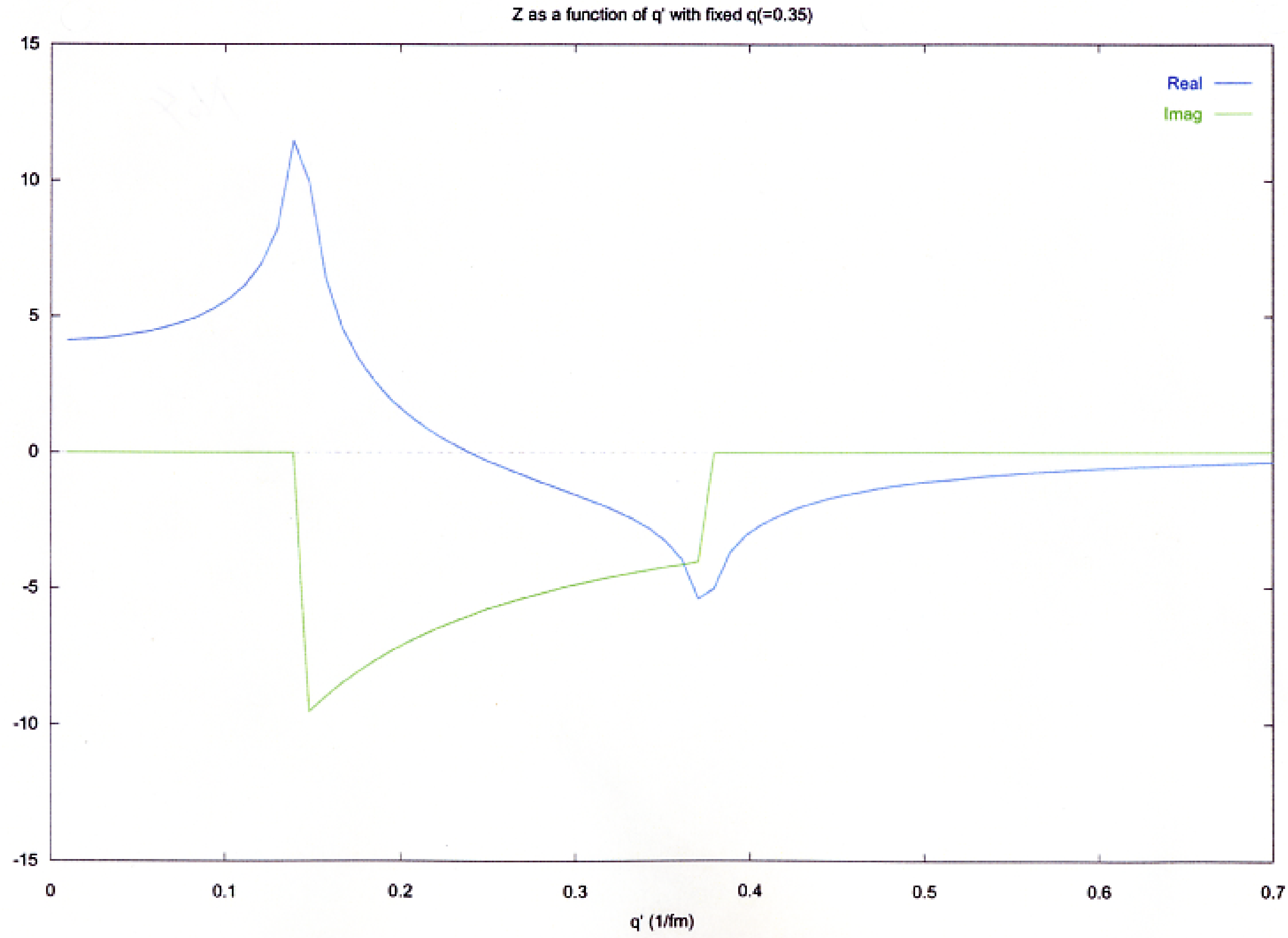
Z as a function of q' with fixed q(=0.35)
Real
Imag
15
10
5
0
-5
-10
-15
0
0.1
0.2
0.3
0.4
0.5
0.6
0.7
q' (1/fm)

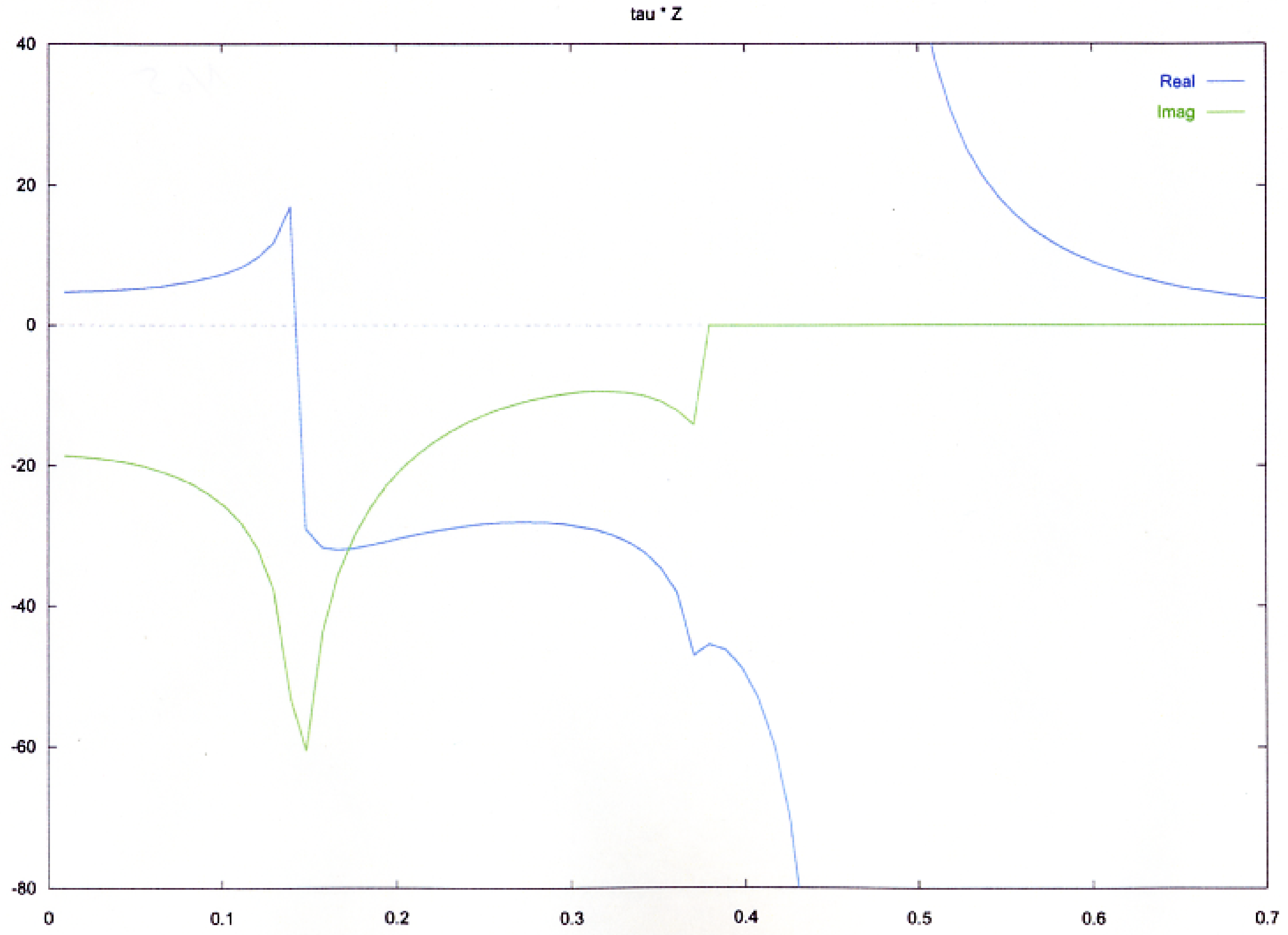
tau * Z
Real
Imag
40
20
0
-20
-40
-60
-80
0
0.1
0.2
0.3
0.4
0.5
0.6
0.7

SUMMARY

In the three-body system, complexity of the threshold depend on the three-body energy.

- below all two-body threshold: no singularity at all only three-body bound states
- At negative energies: two-body singularities elastic scattering and rearrangement scattering
- At positive energies: all singularities elastic, rearrangement and breakup

Singularities reflect the wave function at infinity.

Comment on Coulomb

Coulomb interaction
goes to infinity in coordinate space
or singular in the momentum space.

That is why Coulomb interaction is difficult to treat.

However, there is no problem for bound states:
because no singularity from the wave function.

It is relatively easy below the breakup threshold.

Extremely difficult above the breakup threshold($E > 0$).

Introduction to three-nucleon studies

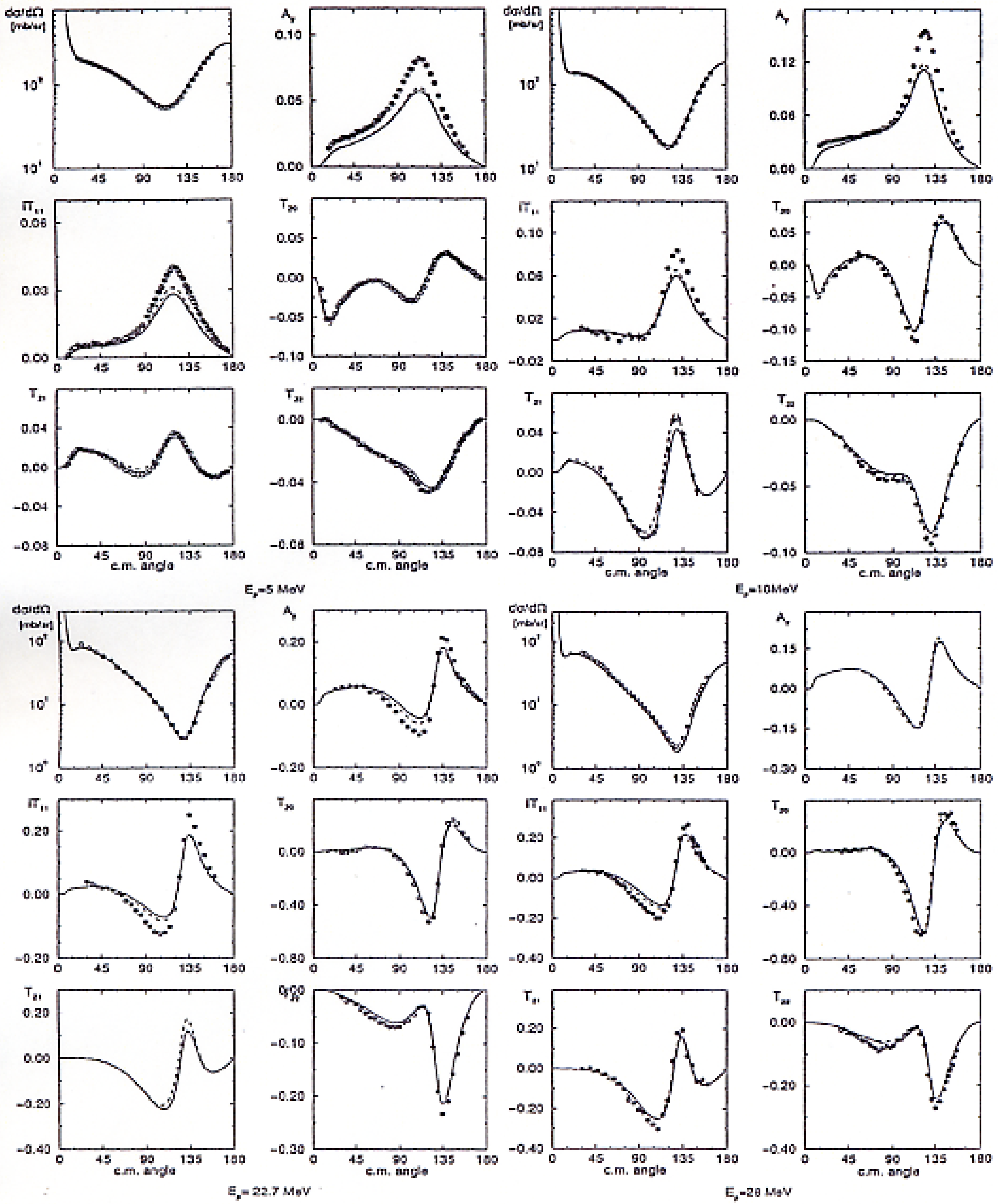

Figure 1. Differential cross section, vector and tensor analyzing powers calculated using the AV18 potential (solid line) and AV18+UR potential (dashed line). Experimental points are from ref.[7]

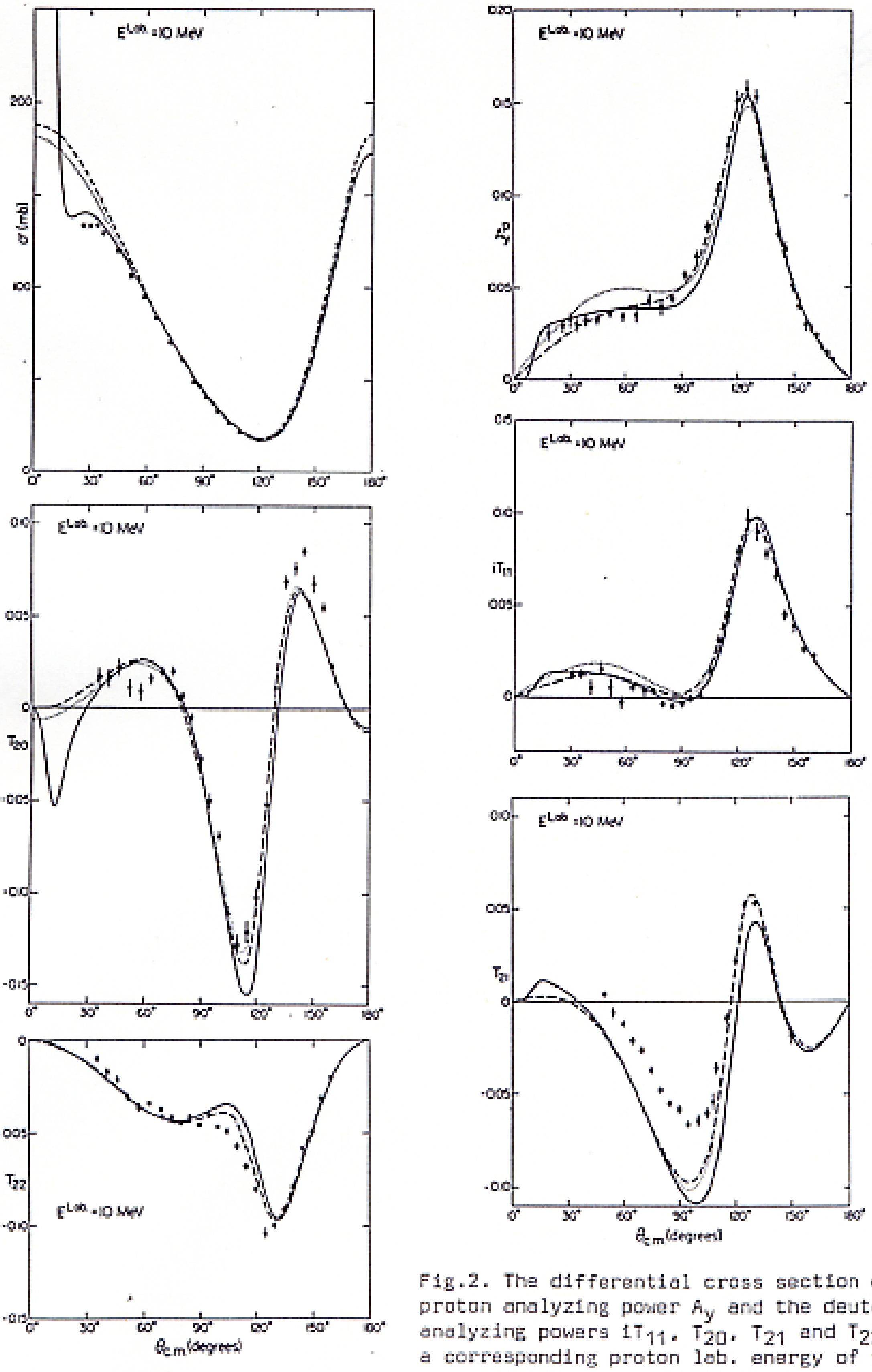

Fig.2. The differential cross section σ, the proton analyzing power A_y and the deuteron analyzing powers iT_{11}, T_{20}, T_{21} and T_{22} for a corresponding proton lab. energy of 10 MeV. The curves are the results of Faddeev calculations.

Few-Body Conference at Eugene 1980.

Nuclear Interactions (Primitive models)

- Square well potential
- Gaussian potential
- Woods-Saxon potential
- Separable potential

These potentials are easy to treat.
Parameters are fitted phenomenologically.

Nucleon-Nucleon Interaction

The interaction is obtained with a certain theory and fitted to the existing two-nucleon data precisely.

(background theory and accurate phenomenology)

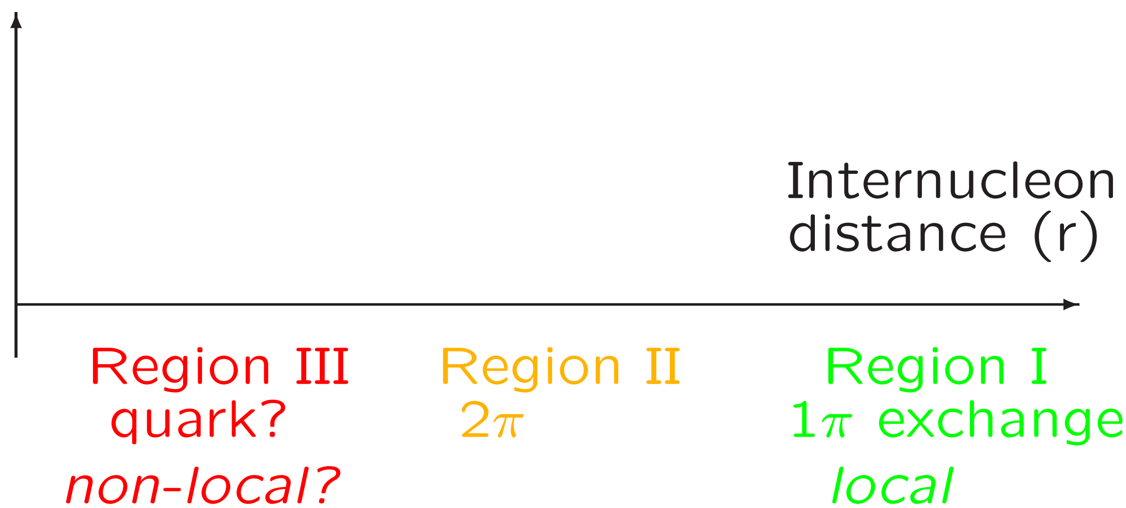

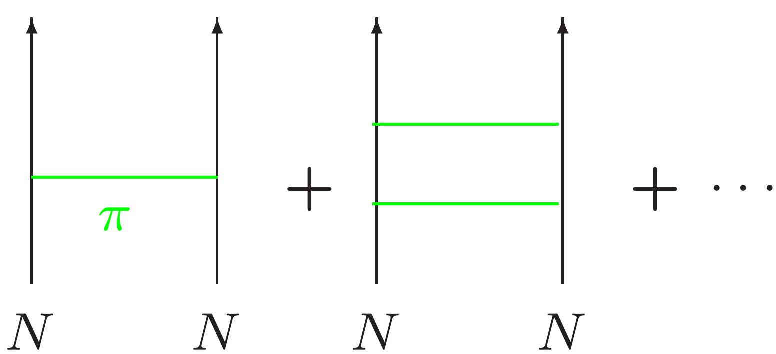

OBE(One Boson Exchange) potential

The interaction obtained with a basic idea
that Region II and III
are described by exchanging heavier bosons.

Reid93

AV18

Njimegen I, II

CD Bonn

etc.

In these interactions, parameters are fitted
to describe phase shifts
and observed two-nucleon experiments

below pion production threshold extremely well

($\chi^2 \approx 1$).

for instance, refer to
http://nn-online.sci.kun.nl/

Some New Attempts

- Effective perturbation theory in Region II and III
- Quark RGM in Region III

Region I

Central + Strong Tensor.

YUKAWA theory: Interaction established only here

Strong tensor: The deuteron d-state, and low energy ^3p_J Phases.

Region II

Not only central, but Spin-Spin, Spin-Orbit, and more complicated operators.

Attractive at least even parity.

Attractive: deuteron in $^3s_1$-$^3d_1$, virtual state in $^1s_0$
1π exchange is not attractive enough in these states.

Region III

Essentially repulsive

$^1s_0$ and $^3s_1$ phases are negative at higher energy.

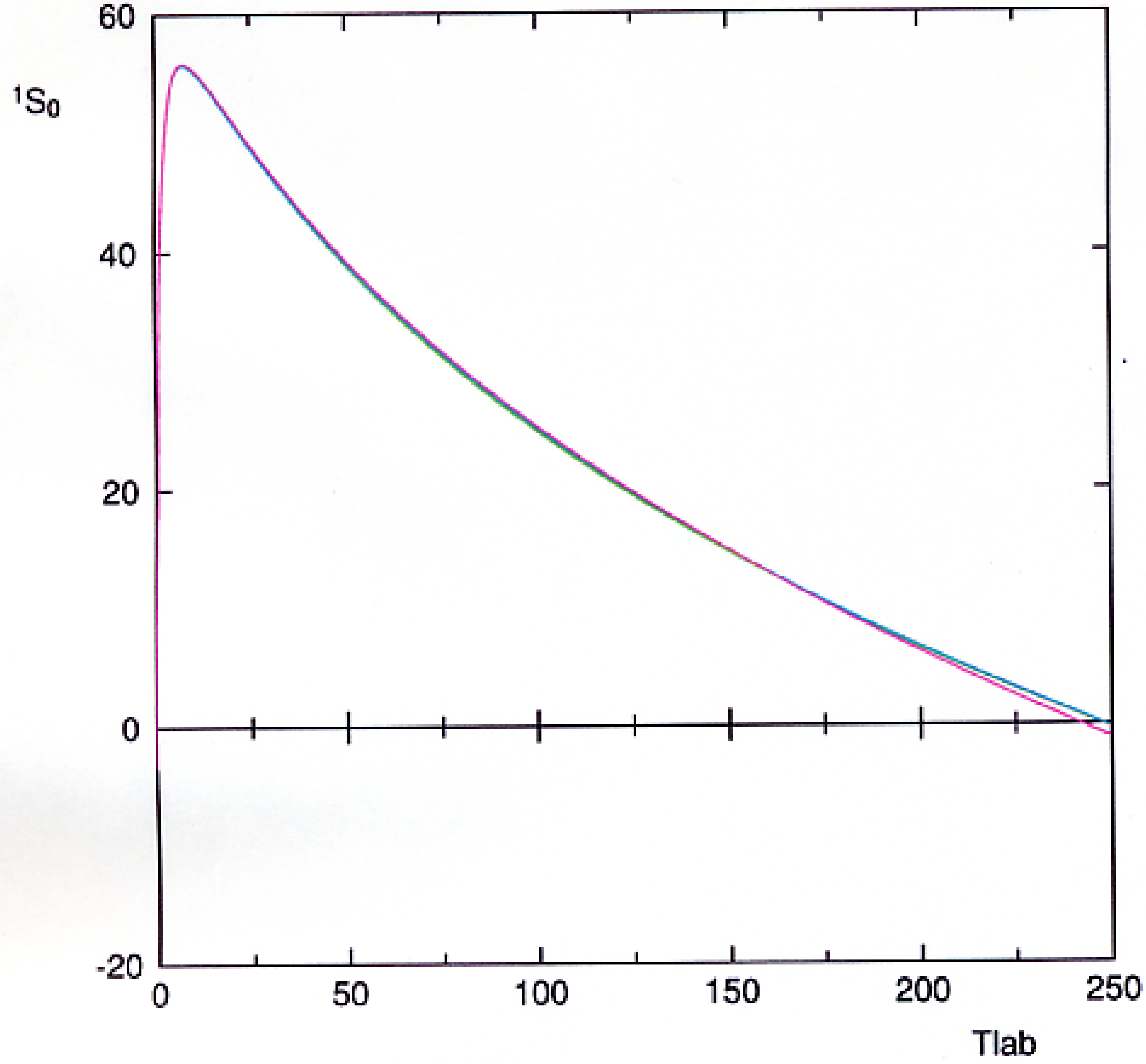

pp phaseshift $^1S_0$

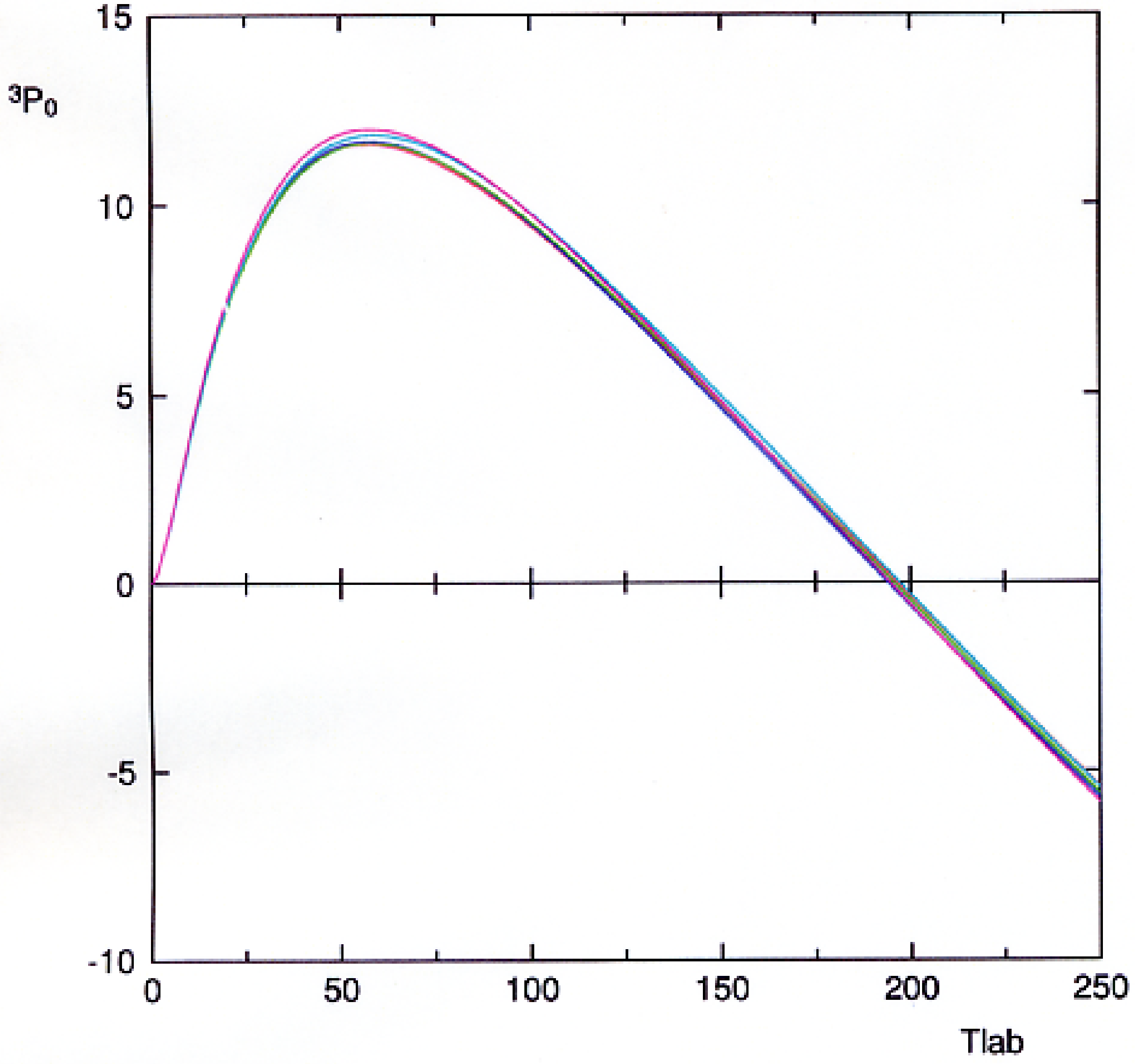

pp phaseshift $^3P_0$

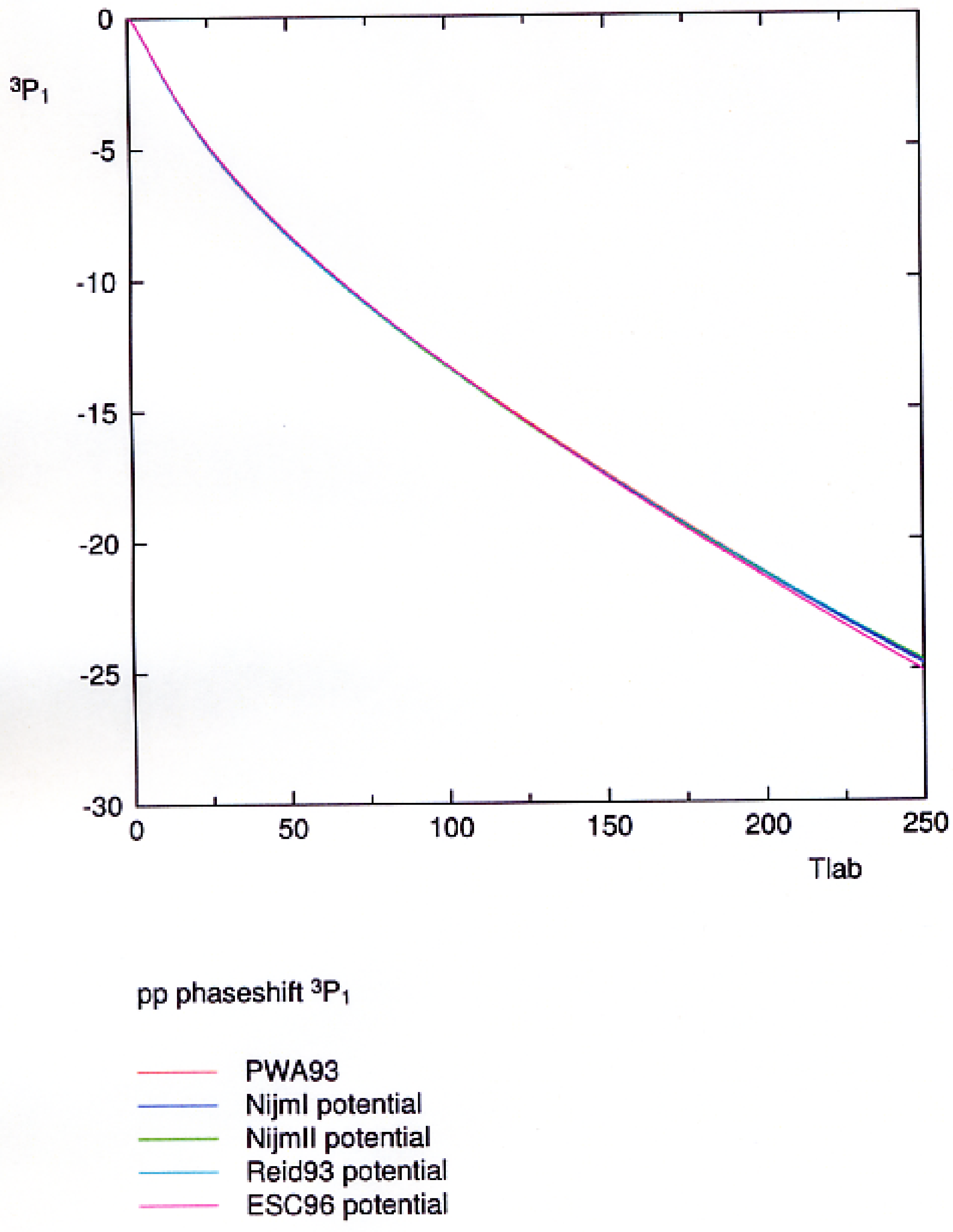

NN-OnLine http://nn-online.sci.kun.nl 15 August 2002

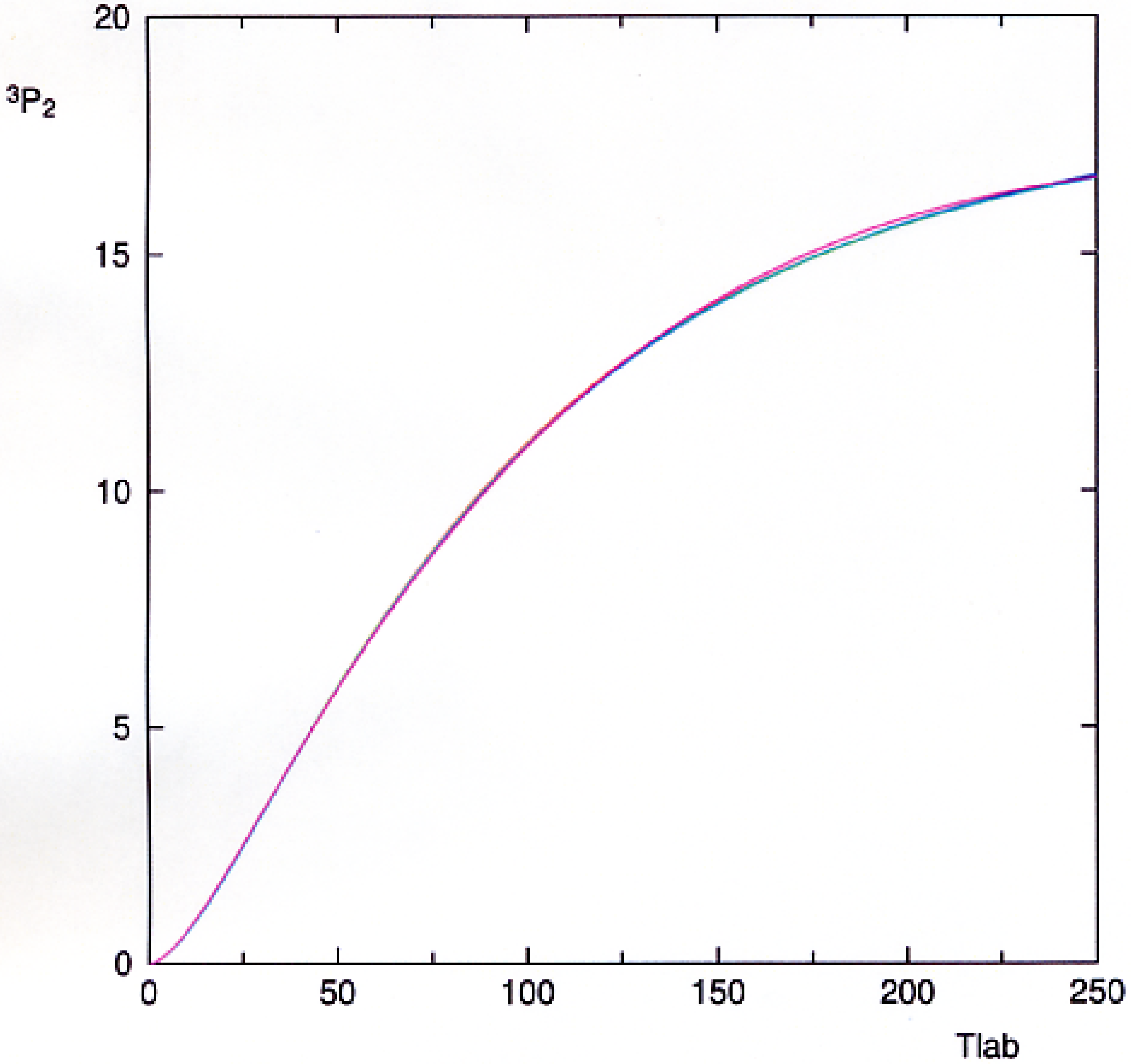

pp phaseshift $^3P_2$

PWA93
NijmI potential
NijmII potential
Reid93 potential
ESC96 potential

NN-OnLine http://nn-online.sci.kun.nl 15 August 2002

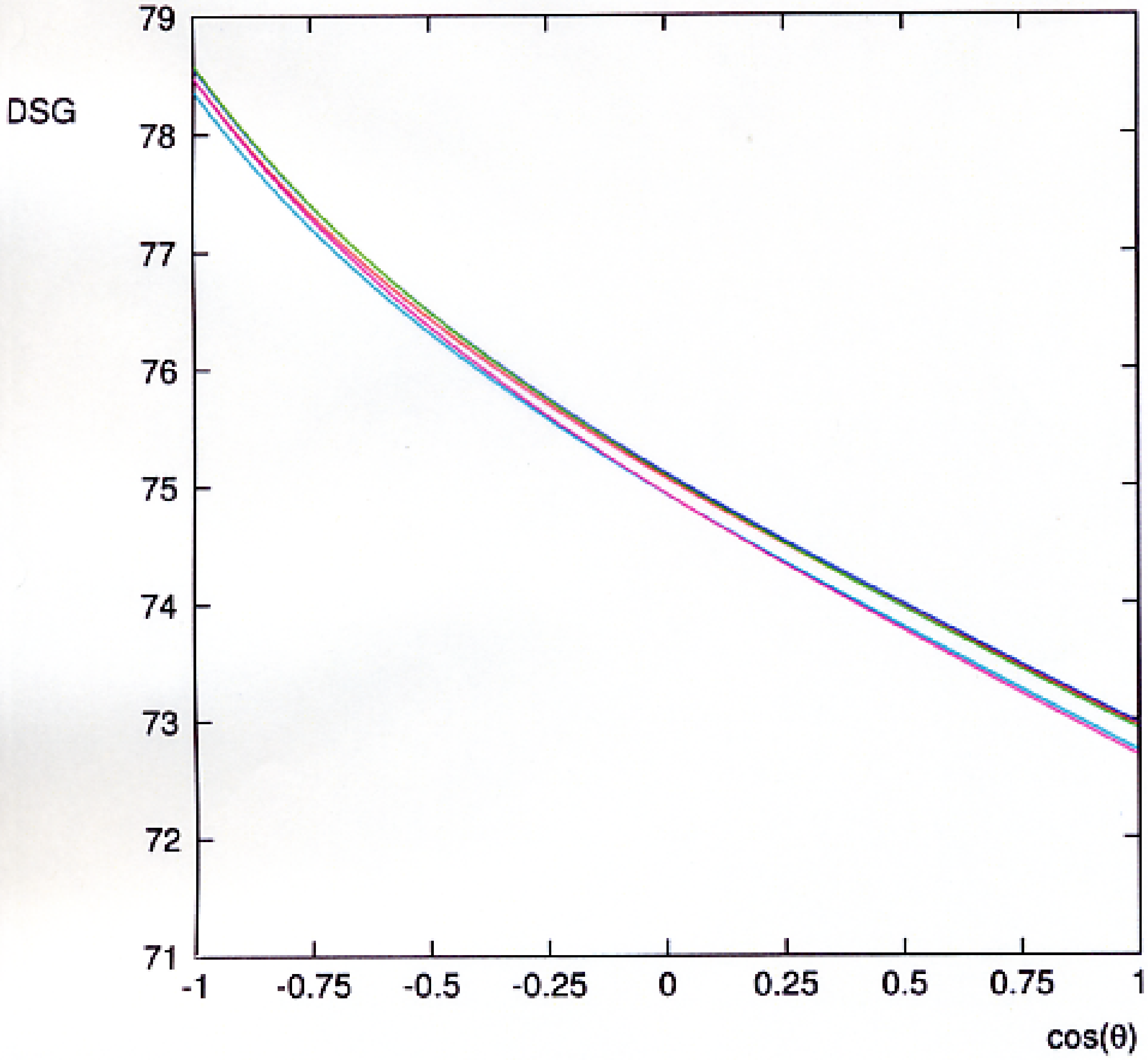

np observable DSG at Tlab = 10.0 MeV

- PWA93
- NijmI potential
- NijmII potential
- Reid93 potential
- ESC96 potential

TABLE I. $3N$ binding energies E_B for different NN interactions compared to the experimental values. Results are shown for ^3H, ^3He and their binding energy difference ΔE_B. Additionally, we show the kinetic energies T. All results are given in MeV.

	^3H		^3He		
Interaction	E_B	T	E_B	T	ΔE_B
CD-Bonn	−8.013	37.43	−7.288	36.62	0.725
AV18	−7.628	46.76	−6.917	45.69	0.711
Nijm I	−7.741	40.74	−7.083	40.01	0.658
Nijm II	−7.659	47.55	−7.008	46.67	0.651
Nijm 93	−7.668	45.65	−7.014	44.79	0.654
Expt.	−8.482		−7.718		0.764

TABLE II. $3N$ binding energy results for different combinations of NN and $3N$ interactions, together with the adjusted form factor parameters Λ in units of m_π. The binding energies for ^{3}H $E(^3\text{H})$ and ^{3}He $E(^3\text{He})$ are shown. For completeness, the splitting ΔE_B is also displayed. All energies are given in MeV.

Interaction	Λ	$E(^3\text{H})$	$E(^3\text{He})$	ΔE_B
CD-Bonn+TM	4.784	−8.478	−7.735	0.743
AV18+TM	5.156	−8.478	−7.733	0.744
AV18+TM'	4.756	−8.448	−7.706	0.742
AV18+Urb-IX		−8.484	−7.739	0.745
AV18+Urb-IX (Pisa) [69]		−8.485	−7.742	0.743
AV18+Urb-IX (Argonne) [28]		−8.47(1)		
Expt.		−8.482	−7.718	0.764

'on value, Eq. (6), deter ined self-consistently.

model	channels	$n_{\max}$	$\varepsilon(2N)$ (MeV)	$E(^3\mathrm{H})$ (MeV)	$\sqrt{\langle r^2\rangle_{^3\mathrm{H}}}$ (fm)	$\sqrt{\langle r^2\rangle_{^3\mathrm{He}}}$ (fm)
	2 ch	2,100	2.361	−7.807	1.80	1.96
	5 ch	5,250	4.341	−8.189	1.75	1.92
fss2	10 ch	10,500	4.249	−8.017	1.76	1.94
	18 ch	18,900	4.460	−8.439	1.72	1.90
	34 ch	35,700	4.488	−8.514	1.72	1.90
	2 ch	2,100	2.038	−7.674	1.83	1.99
	5 ch	5,250	3.999	−8.034	1.78	1.95
FSS	10 ch	10,500	3.934	−7.909	1.78	1.97
	18 ch	18,900	4.160	−8.342	1.74	1.93
	34 ch	35,700	4.175	−8.390	1.74	1.92

Y. Fujiwara et al. PRC 66('02)

Table: Typical calculated total cross sections in n-d scattering. The cross sections are in mb. Potential used is AV14, but all OBE two-body potential would give similar result. Note that the breakup process is definitely more important at higher energy.

E^{lab}	10 MV	30 MV	70 MV	100 MV	135 MV
elastic	912	230	43	31.5	18.7
b-up	142	123	82	61.4	53.4
total	1054	353	142	92.9	72.1

Table: The same as the table above but with the contribution ratio (quartet/doublet) is given in the parenthesis. Here, quartet means the quartet induced cross section. If it were just central interactions, the ratio would be 2.

E^{lab}	10 MV	70 MV	135 MV
elastic	912 (4.6)	43 (2.5)	18.7 (3.9)
b-up	142 (0.4)	82 (1.8)	53.4 (2.8)

.E II. Total n-d cross section calculated from the Paris
l in comparison to experimental data.

V)	σ_{calc} (mb)	σ_{expt} (mb) Ref. 40	Ref. 41
	1469	1478±16[a]	1471±20
	1330	1296±10[a]	1337±10
	1225	1207±13	1224±10
	1129	1118±10[a]	1128±10
	1047	1055±10	
	1028		1038±10
	912	913±13	923±10
	807		824±10
	650		666±7
	587	584±10[a]	603±6

xperiments are at slightly different energies $\Delta E_n \approx \pm 0.1$

Y. Koike, J. Haidenbauer and W. Plessas, PRC 35 (1987) 396

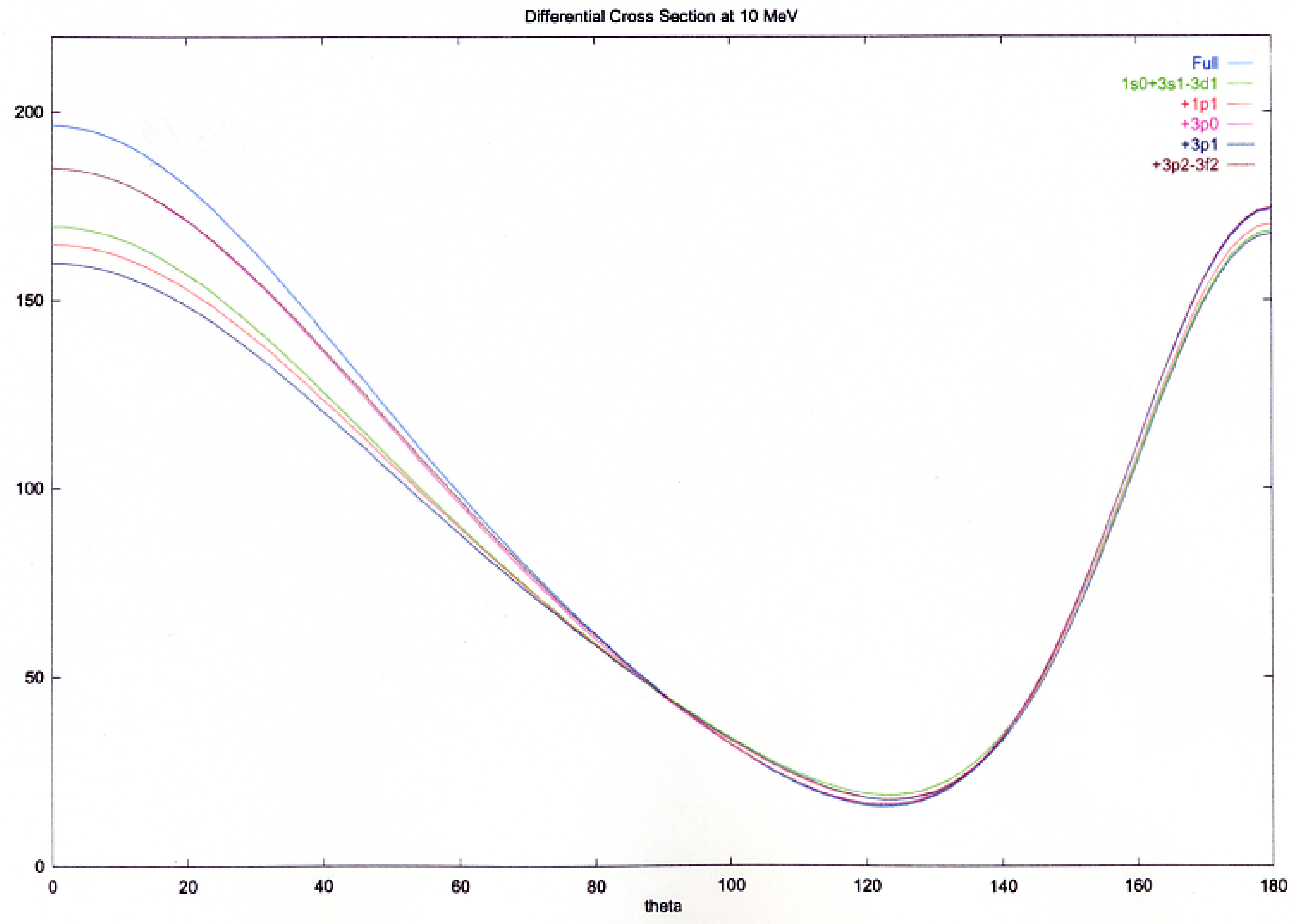
Differential Cross Section at 10 MeV
Full
1s0+3s1-3d1
+1p1
+3p0
+3p1
+3p2-3f2
0
50
100
150
200
0
20
40
60
80
100
120
140
160
180
theta

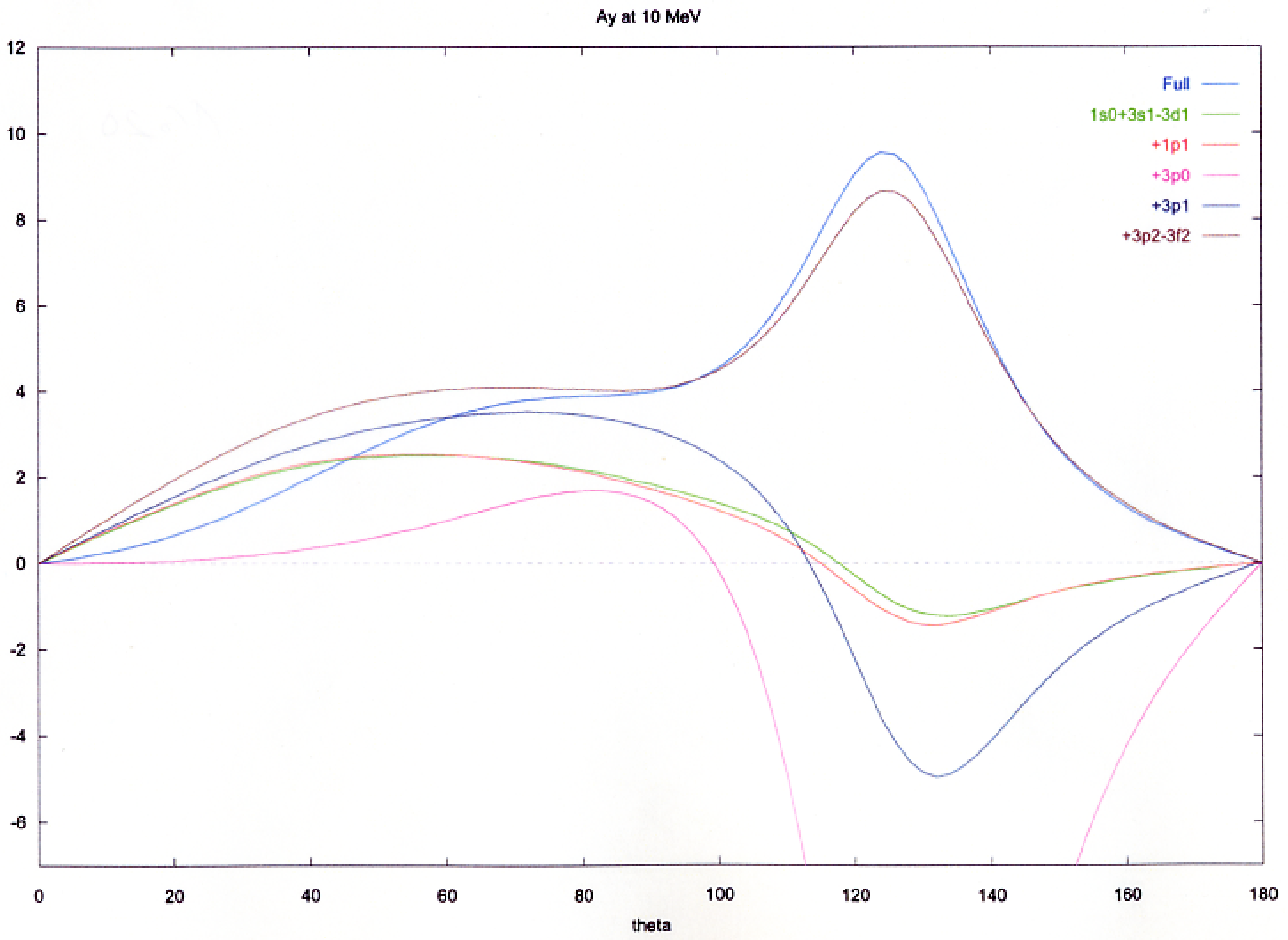

Ay at 10 MeV
Full
1s0+3s1-3d1
+1p1
+3p0
+3p1
+3p2-3f2
12
10
8
6
4
2
0
-2
-4
-6
0
20
40
60
80
100
120
140
160
180
theta

The main purpose of N-d scattering study

To examine if internucleon potentials,

like OBE

are enough describing nuclear phenomena

What is missing

The three-body force

An important concept

The off-shell effect

$\Downarrow$

The main purpose of N-d scattering study

Investigate three-body force in detail,

taking care of the off-shell effect.

variety of methods have been used in momentum space, configuration space, and a combination of these spaces to obtain eigenvalues for a diverse set of realistic nucleon-

iltonian, the nonrelativistic trinucleon bound lem appears to be well under control.

In contradistinction, three-nucleon scatter

TABLE I. Spin-doublet results.

	Utrecht	Jülich/NM	Bochum	LA/Iowa	Hosei
		E=4.0 MeV (lab)			
Re(δ)	143.7	143.7	143.7	143.7	143.7
η	0.963	0.952	0.964	0.964	0.964
		E=14.1 MeV (lab)			
Re(δ)	106.5	104.9	105.5	105.4	105.5
η	0.468	0.460	0.467	0.463	0.465
		E=42.0 MeV (lab)			
Re(δ)	41.9	41.3	41.3	41.2	41.3
η	0.488	0.501	0.504	0.501	0.502

TABLE II. Spin-quartet results.

	Utrecht	Jülich/NM	Bochum	LA/Iowa	Hosei
		E=4.0 MeV (lab)			
Re(δ)	102.1	101.1	101.6	101.5	101.6
η	1.000	1.000	0.999	1.000	1.000
		E=14.1 MeV (lab)			
Re(δ)	68.8	68.5	69.0	68.9	68.9
η	0.978	0.986	0.978	0.978	0.978
		E=42.0 MeV (lab)			
Re(δ)	38.4	37.2	37.7	37.8	37.7
η	0.898	0.907	0.903	0.906	0.903

First Benchmark solution

The same potential, different method

Utrecht : two dimensional integral eqs. in mom. sp.

Bochum : "

Julich / NM : separable EST

Hosei : " orthogonal basis

LA / Iowa : coordinate space

PRC 42 (1990) 1838

A Three-Body Interaction

Any three-nucleon diagram which can not be reduced to a sum of two-nucleon process is a three-body interaction

Simple and probably most important process: two-pion process with

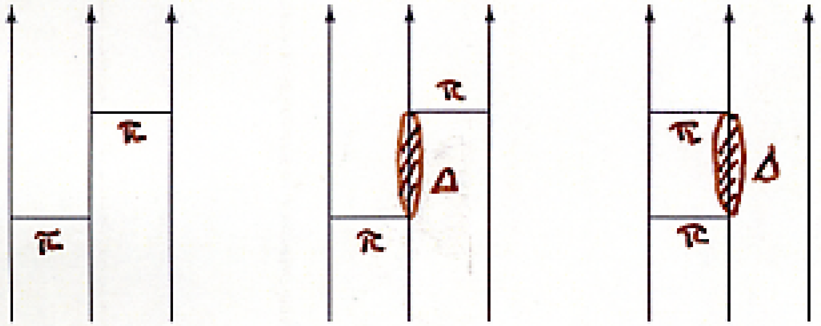

Successive 2-BI 3-BI 2-BI

This three-body interaction should be important at the cross section minimum at higher energies, because

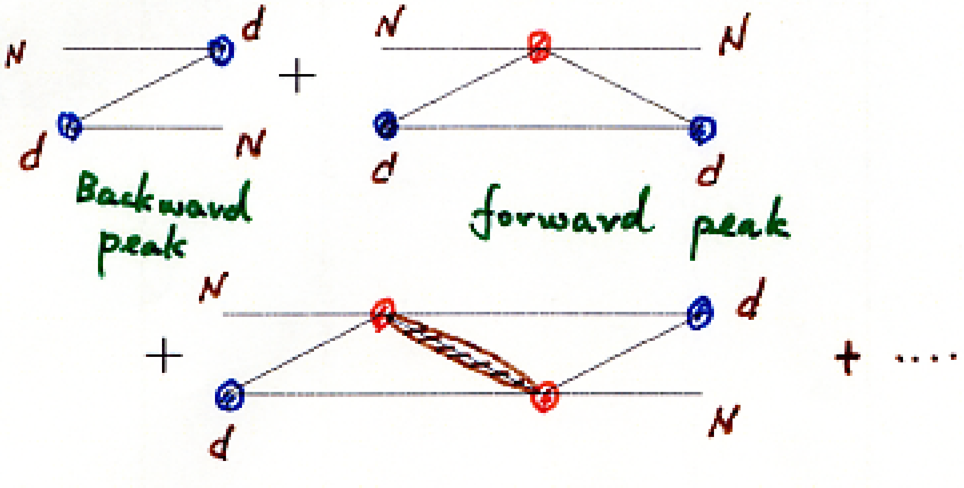

.reated
: intro-

. struc-
igs. 10
in the
oduced
. How-
At in-
section
whole
ulation
iment,
: in the
oulomb
ement.
s been
Zankel
tion is
culated
t back-
e same
angles
y from
, while
l to in-
nuclear

: $\vec{p}+d$

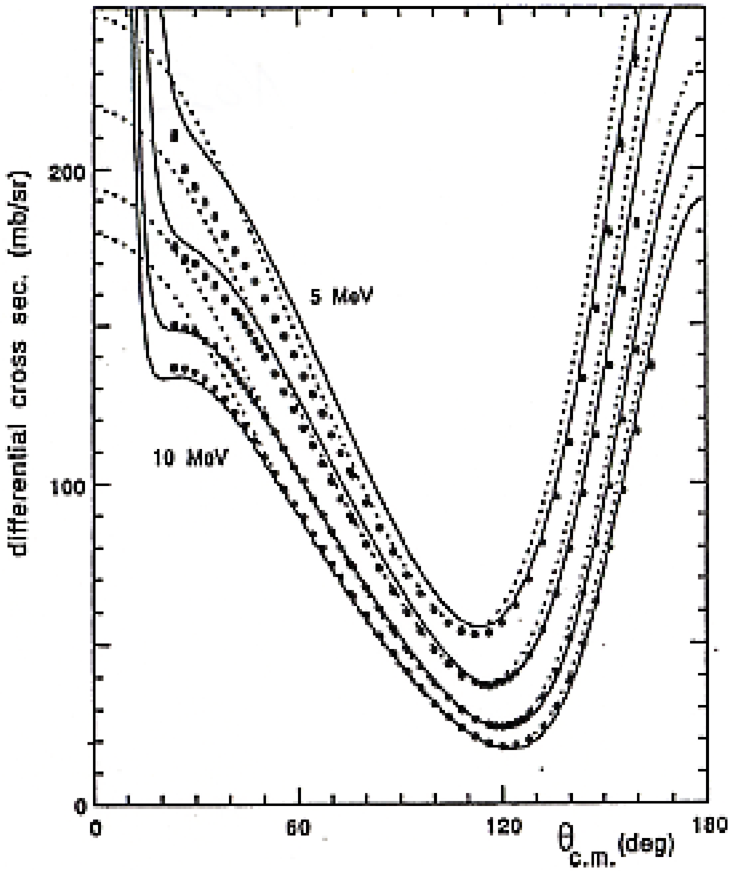

FIG. 10. Differential cross section in the $p+d$ scattering at $E_p = 5$ (top), 6.5, 8.5, and 10 MeV (bottom). The solid (dashed) curves are the results of the Faddeev calculation Ref. [16] for the $p+d$ ($n+d$) scattering using the Paris NN potential.

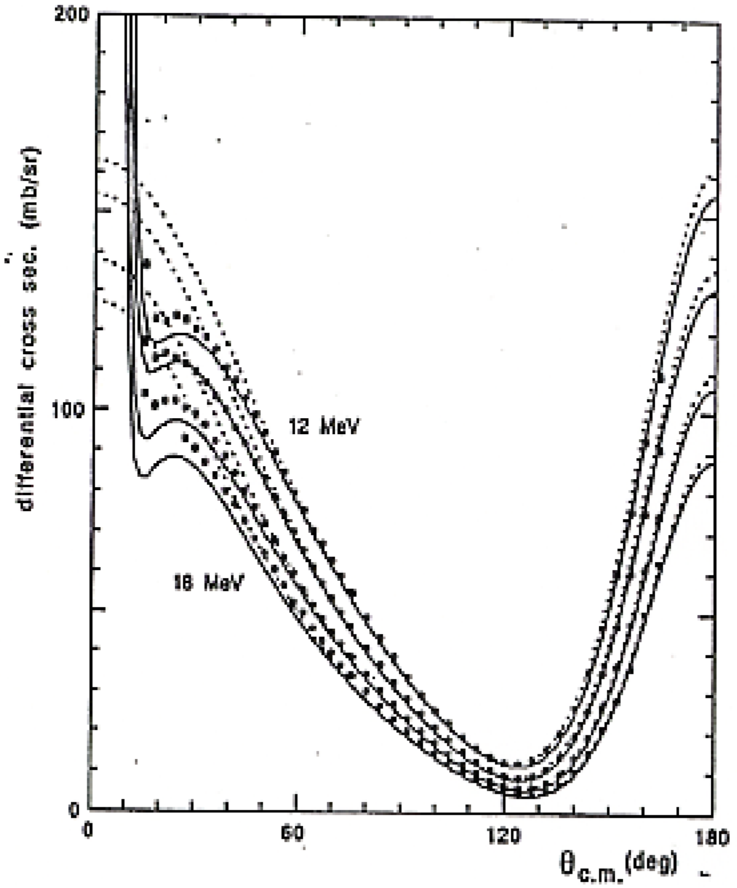

FIG. 11. The same as in Fig. 10 at $E_p = 12$ (top), 14, 16, and 18 MeV (bottom).

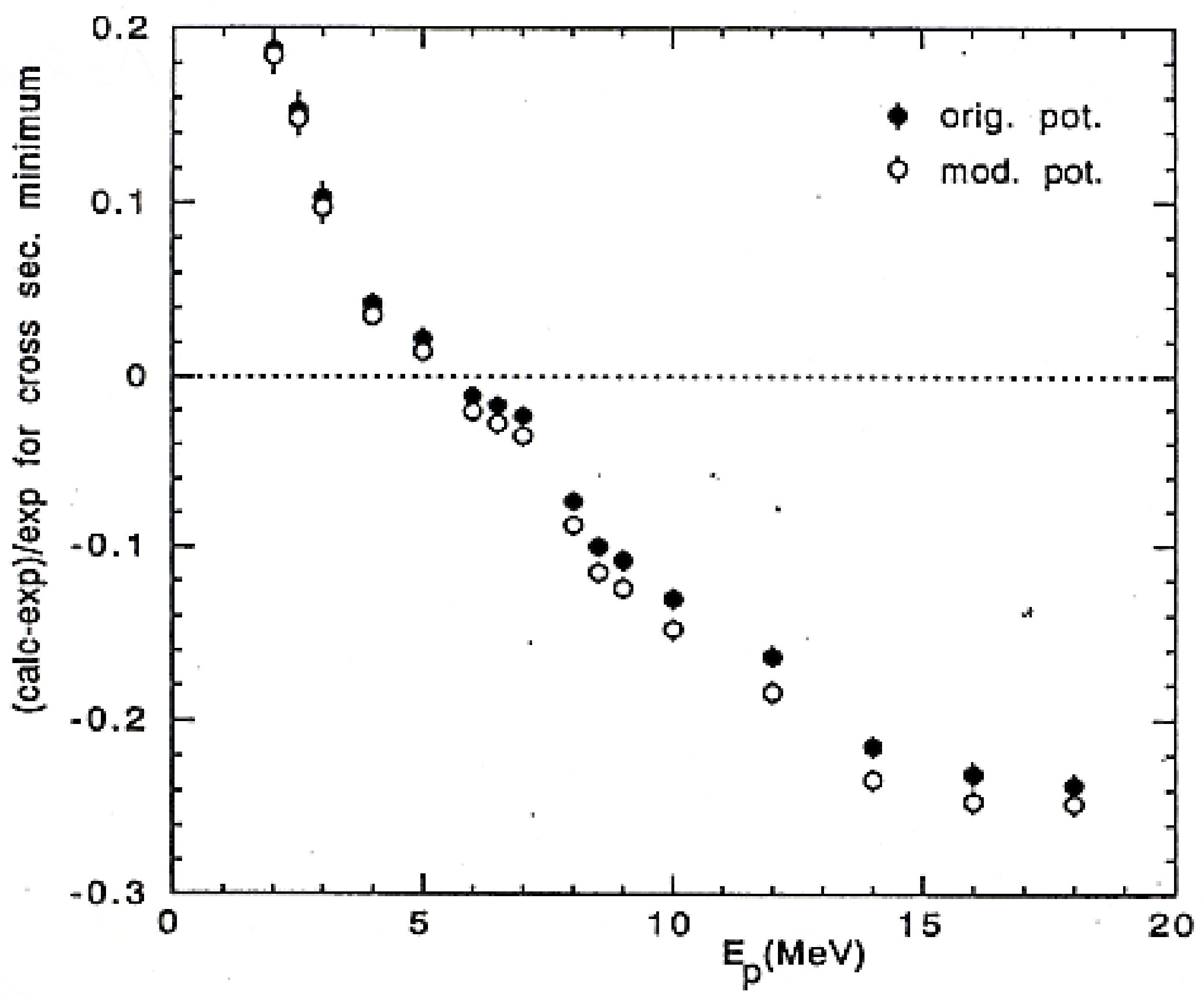

FIG. 17. Fractional discrepancy of the cross-section minimum, $\Delta\sigma = (\sigma^{\rm calc} - \sigma^{\rm exp})/\sigma^{\rm exp}$. The present $p+d$ data are compared with the Faddeev calculations [16] using either the original Paris NN potential (solid circle) or the Paris NN potential whose LS force is modified (open circle).

K. Sekiguchi et al. PRC 65 ('02)

sc..sion

n for the

shown in

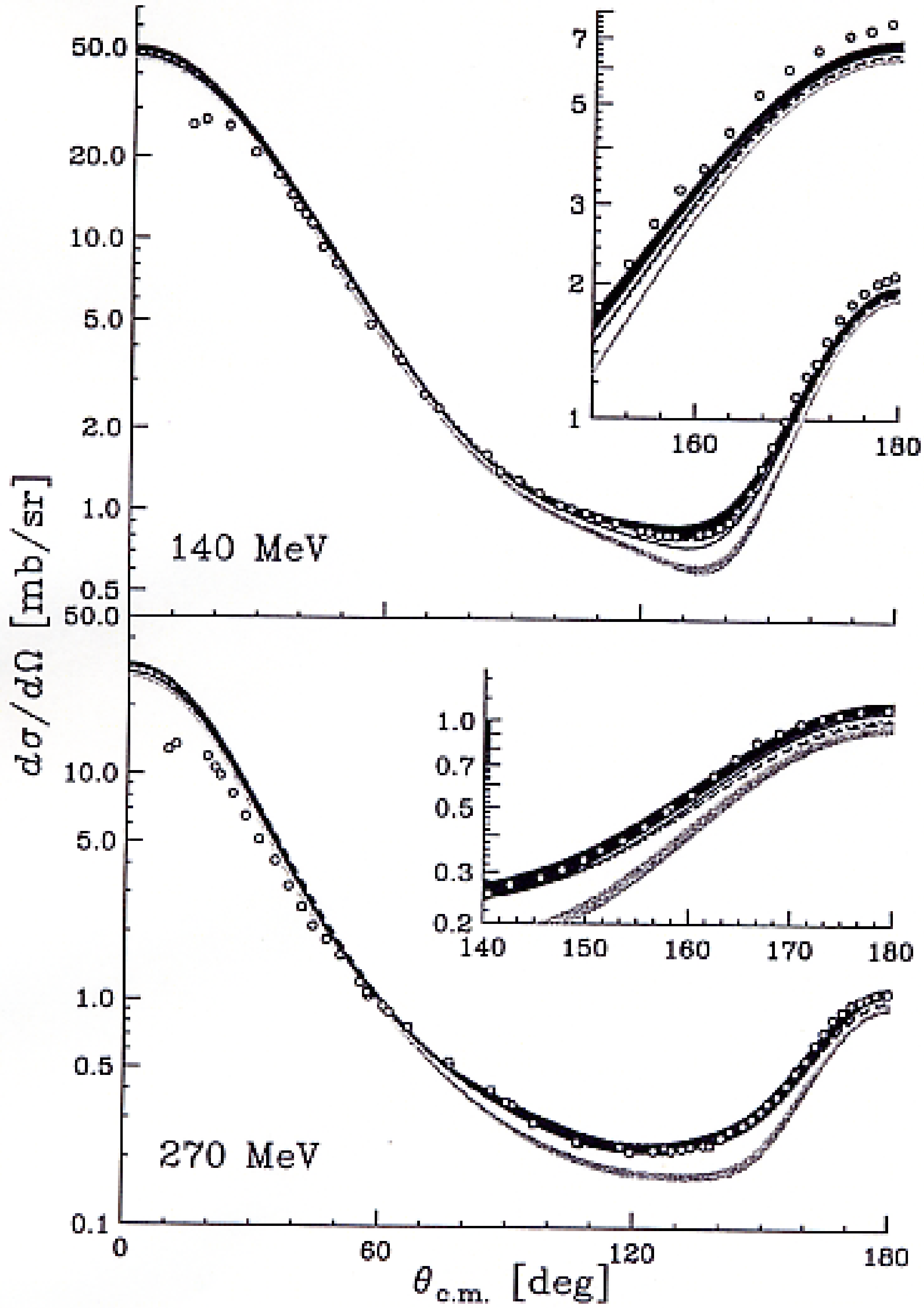

Figure 5.1: The differential cross section $d\sigma/d\Omega$ in elastic Nd scattering at E_d=140 and 270 MeV. The light shaded bands contain NN force predictions (AV18, CD-Bonn, Nijm I, II and 93), the dark shaded bands contain the NN + TM 3NF predictions. The solid, short dashed and long dashed lines are the AV18 + Urbana IX, CDBonn + TM′, and AV18 + Urbana IX + phenomenological spin-orbit 3NF predictions, respectively.

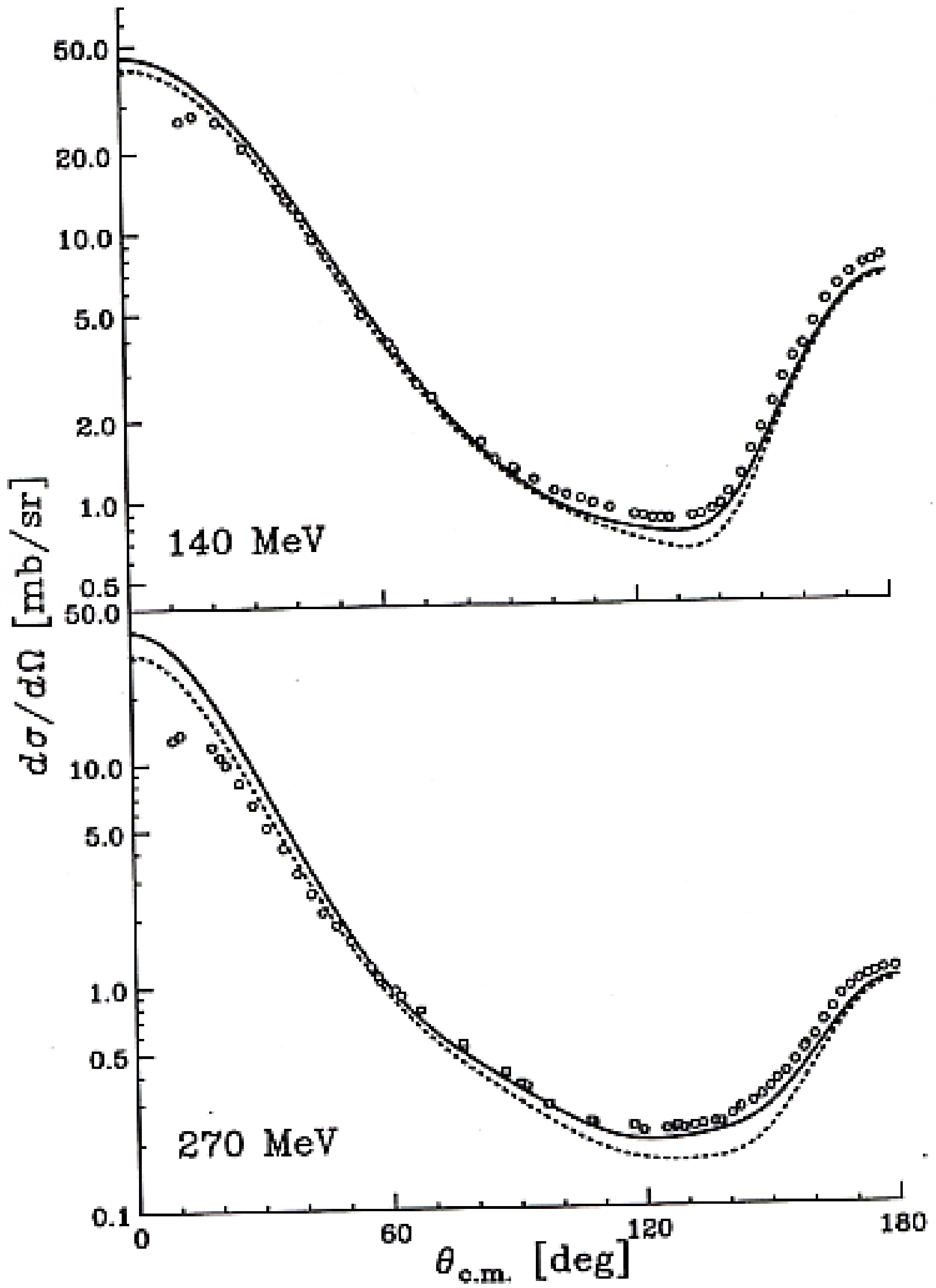

Figure 5.9: The differential cross section $d\sigma/d\Omega$ in elastic Nd scattering at E_d=14(and 270 MeV. The thick solid lines are the predictions with Δ-isobar excitatior and the thick dotted lines contain 2N force predictions based on Paris Potential.

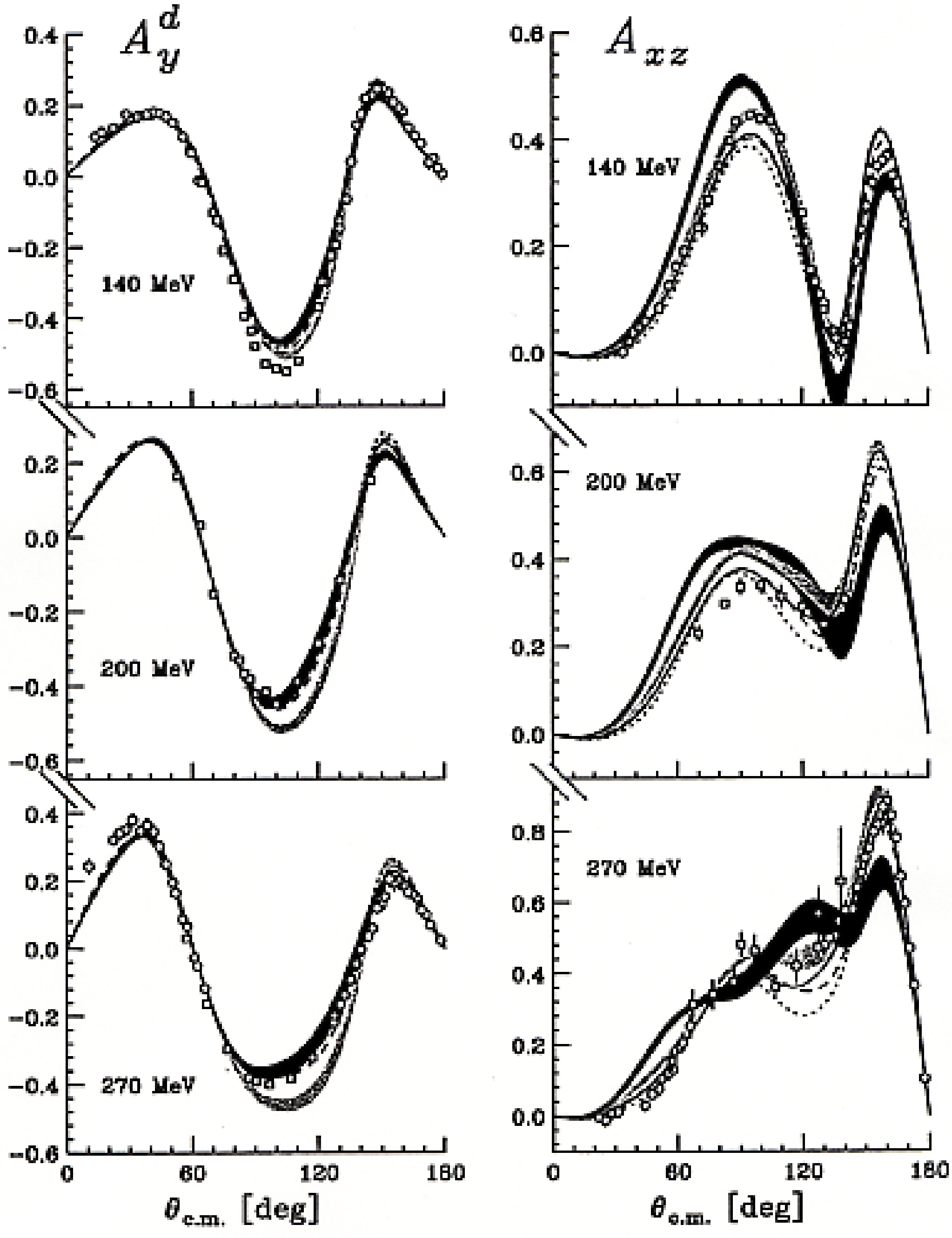

Figure 5.2: The vector analyzing power A_y^d and the tensor analyzing power A_{xz} in elastic Nd scattering at E_d=140, 200, and 270 MeV. For the description of bands and curves see Fig. 5.1.

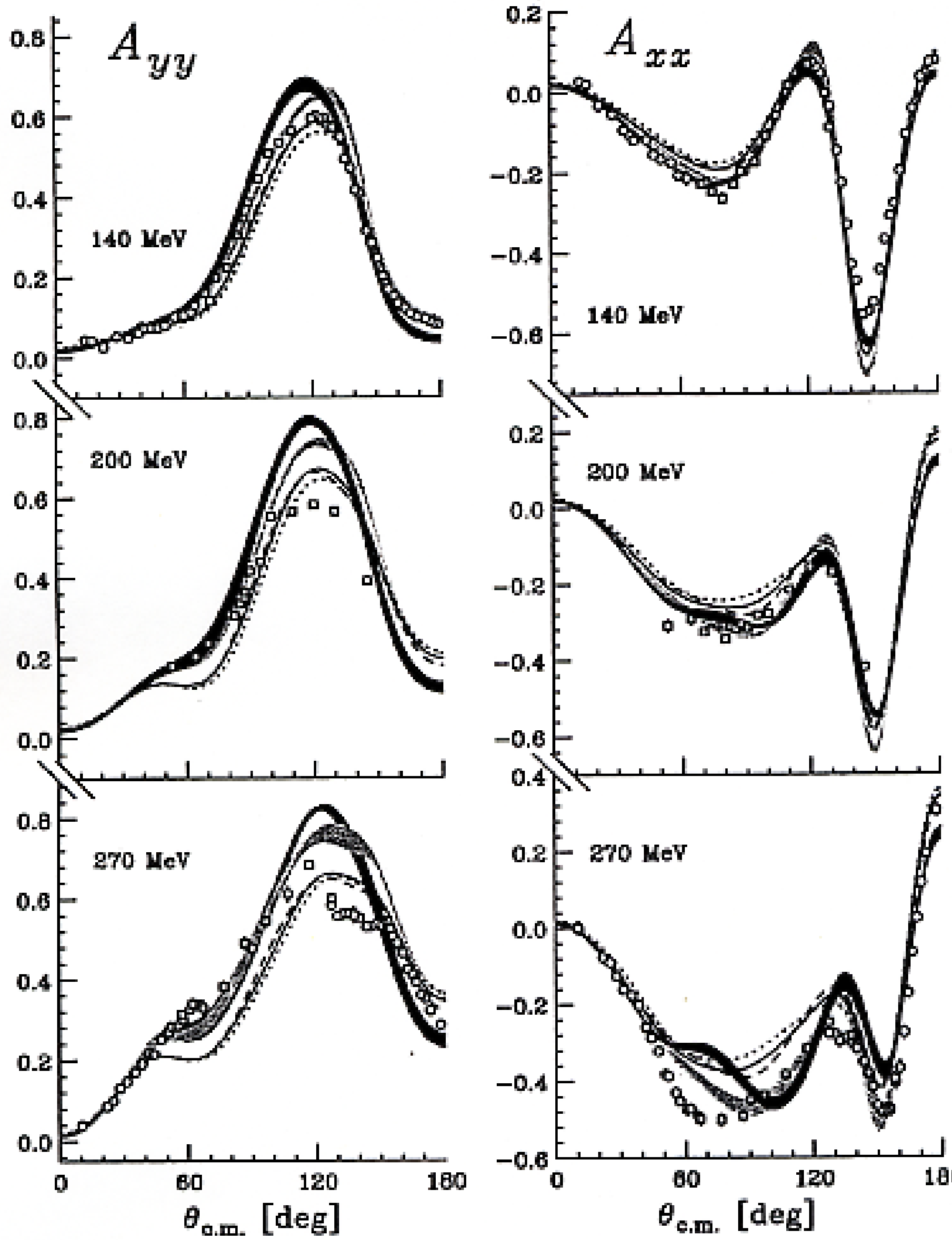

Figure 5.3: The tensor analyzing powers A_{yy} and A_{zz} in elastic Nd scattering at E_d=140, 200, and 270 MeV. For the description of bands and curves see Fig. 5.1.

5.3 Summary of Comparison : Result for the d–p data and Theoretical Predictions

By comparing the present d–p elastic scattering data with the theoretical predictions, we can categorize the observables into the three types.

Type I : $d\sigma/d\Omega$, A_y^d, $K_{xx}^y - K_{yy}^{y'}$

For these observables, the clear discrepancies exist between the data and the 2N force predictions, especially in the angular range where the cross section take minimum. The deviations are explained beautifully by inclusion of 3NFs. All 2π-exchange 3NF potentials considered here (TM, TM′, Urbana IX) provide almost the same 3NF effects (magnitude and direction).

Type II : $P^{y'}$ ($= -A_y^p$)

The TM′ 3NF as well as Urbana IX 3NF describes well the difference between the data and the 2N force predictions, however the inclusion of the TM 3NF shift the calculated results to the right direction but too much. The c–term of the TM 3NF which should not exist under the chiral perturbation theory might be the origin of the wrong 3NF effect (See Sec. 1).

Type III : A_{xx}, A_{yy}, A_{xz}, $K_y^{y'}$, $K_{xz}^{y'}$

No calculation has its superiority for these observables. Although large effects of 3NFs are predicted at the angles $\theta_{c.m.} = 90° - 120°$, they are not at all supported by the data. It is interesting to note that the TM′ and Urbana IX 3NFs provide very similar effects. On the other hand, the 3NF effects by the TM 3NF are quite different from those by the TM′ and Urbana IX 3NFs.

Table 5.6 shows the summary of the result of the comparison for the d–p elastic scattering data. Here we do not mention about the phenomenological SO-3NF, since the inclusion of this 3NF to the AV18 + Urbana IX prediction leads only a minor modification for all measured observables.

Generally, the discrepancies between the data and the 2N force predictions are clearly seen at the angles where the cross sections are in the minimum and they

Y. Satou et al. CNS Preprint

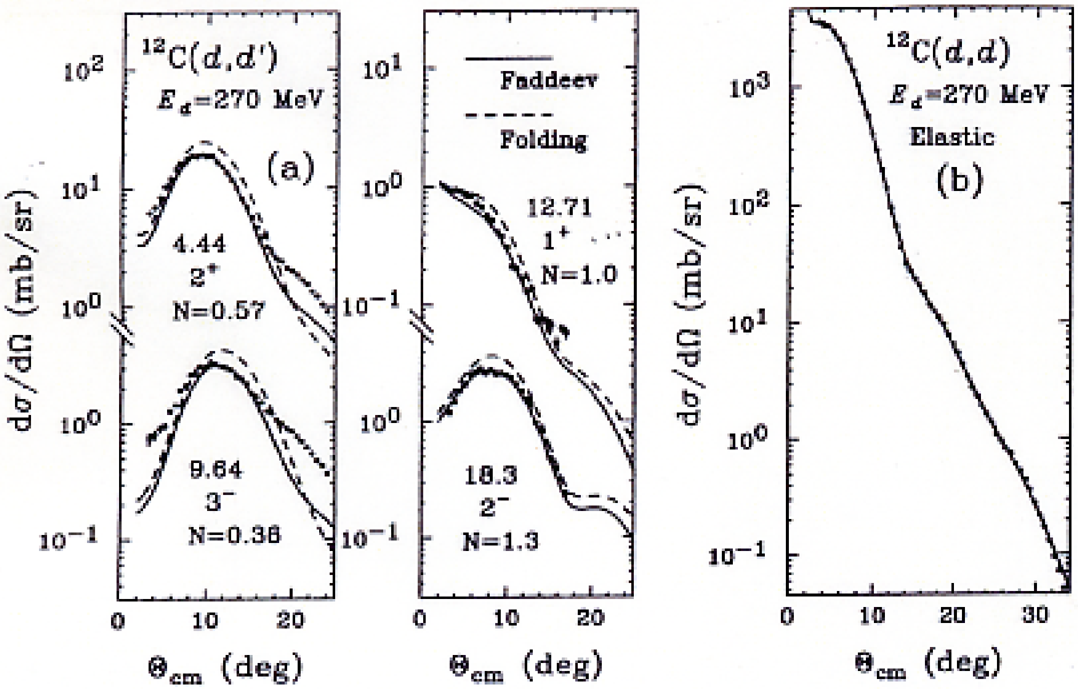

Abstract

We have measured the cross sections and analyzing powers A_y and A_{yy} for the elastic and inelastic scattering of deuterons from the 0^+(g.s.), 2^+(4.44 MeV), 3^-(9.64 MeV), 1^+(12.71 MeV), and 2^-(18.3 MeV) states in ^{12}C at an incident energy of 270 MeV. The data are compared with microscopic distorted-wave impulse approximation calculations where the projectile-nucleon effective interaction is taken from the three-nucleon t-matrix given by rigorous Faddeev calculations presently available at intermediate energies. The agreement between theory and data compares well with that for the (p, p') reactions at comparable incident energies/nucleon.

Key words: (d, d') reaction, DWIA analysis, Three-nucleon t-matrix

[1] E-mail: ysatou@rarfaxp.riken.go.jp

[2] Present address: Soei International Patent Firm, Tokyo 104-0031, Japan.

Preprint submitted to Elsevier Preprint *9 July 2002*

APPLICATIONS OF FEW-BODY METHOD

Especially to hypernuclei and unstable nuclei

It is useful to introduce a three-body model with constituent particles of $N, \Lambda, {}^4$He, ^{9}Li etc.
The direct information from two-body scattering in hypernuclei and unstable nuclei is in many cases hopeless.

Interests are: bound states and resonances.

Typical unstable nuclei: neutron halo.

$$\Downarrow$$

Neutron is weakly bound or
about to bound(but unbound).

Borromean system:

an interesting result from the three-body theory.

Three-body system can be bound even when no subsystems have any bound states.

HOMEWORK EXERCISE

Let us take a three identical boson system. Assuming a simple Yamaguchi separable potential acting just on s-wave

$$V(p, p') = g(p)\lambda g(p') \tag{1}$$

with

$$g(p) = 1/(p^2 + \beta^2) \tag{2}$$

you derive a simple three-body equation(many references).

Keeping β unchanged, you solve two- and three-body equations for bound states. You do not find any bound state for small λ. Potential is too weak. Increasing λ you find:

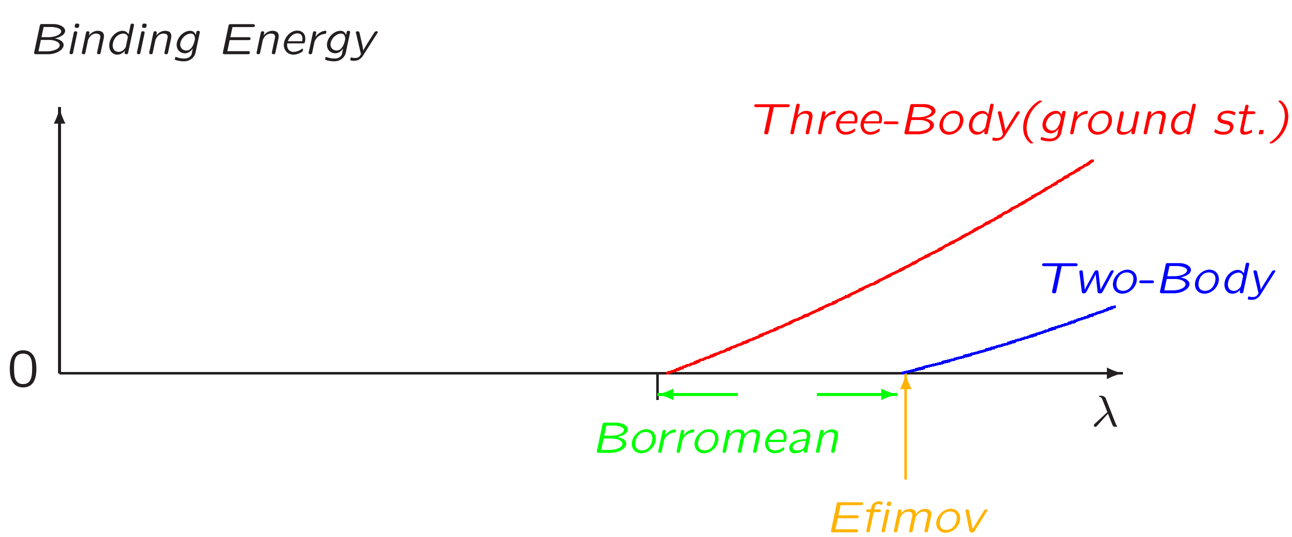

What is more surprising is Efimov states

You can also examine the following theorem as an extended homework:

If the two-body subsystem has a bound state at $E = 0$,

three-identical bosons interacting in s-wave have

infinite numbers of 0^+ bound states. (Efimov)

Example of Borromean system:
^{6}He as n-n-^{4}He system

Example of Efimov states:
He_3, at least two 0^+ states
some unstable nuclei?

I. Mazumdar, V. Arora, and V. S. Bhasin

TABLE III. ^{20}C ground and excited states three-body energy for different two-body input parameters. $\beta_1 = 5.2\alpha$.

n-^{18}C binding energy (keV)	λ_c/α^3	a_s (fm)	ϵ_0 (keV)	ϵ_1 (keV)	ϵ_2 (keV)	N
60	15.51	20.38	3188.03	78.87	65.8	1.01
100	15.89	16.05	3291.54	115.72	100.09	0.94
113.2	16.0	15.15	3317.35	127.41	111.76	0.92
139.60	16.2	13.77	3371.24	150.32	135.29	0.89
168.59	16.4	12.64	3426.03	175.34	163.48	0.86
200	16.6	11.71	3482.95	202.15	194.15	0.84

to reduce the excitation energy to a few keV or corresponding to scattering length to about a hundred fermi that the

Thus,

As an application of the present lecture:

We learn

Two-body potential resonances

$\Downarrow$

Three-body resonances

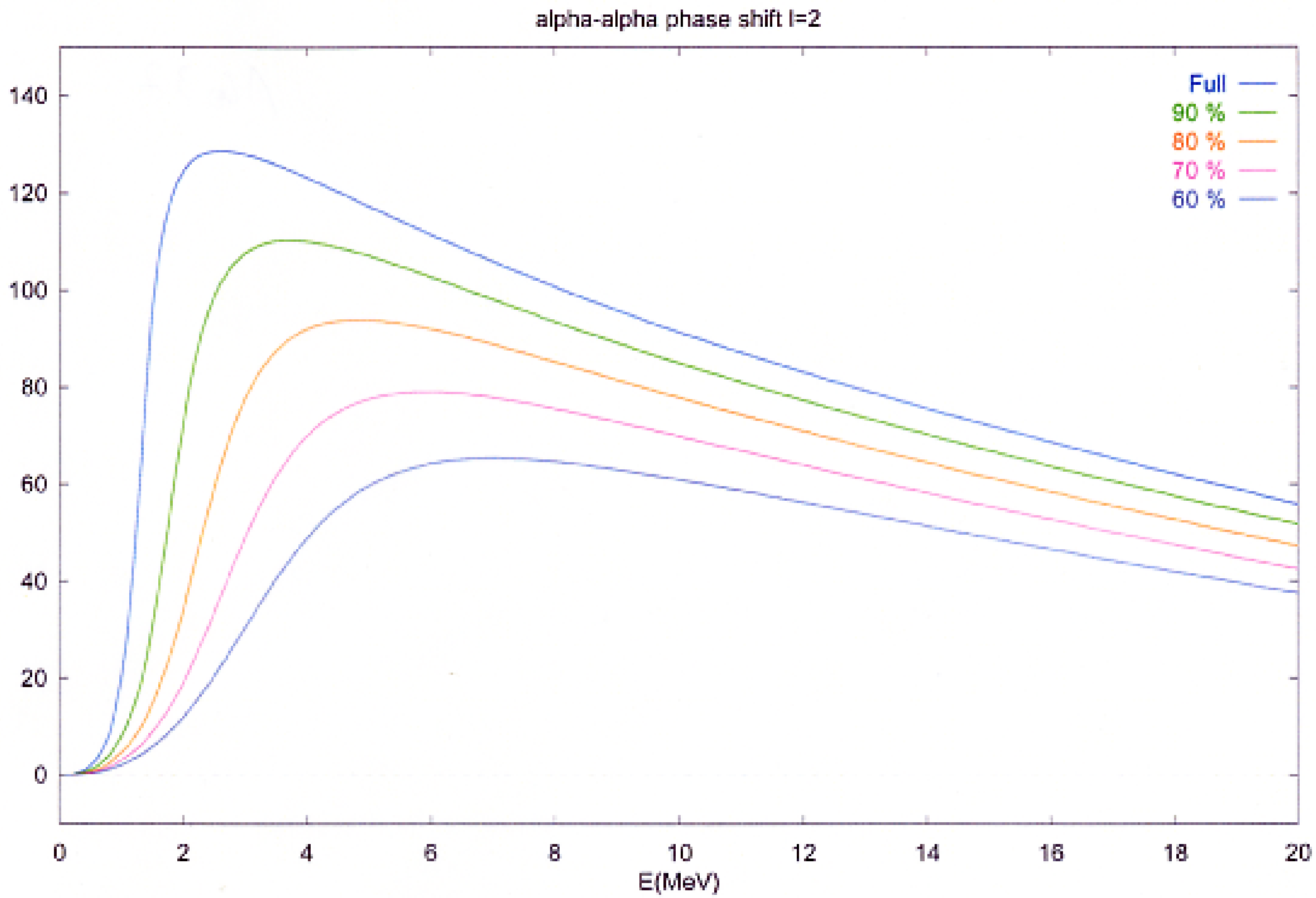
alpha-alpha phase shift l=2
Full
90 %
80 %
70 %
60 %
0
20
40
60
80
100
120
140
0
2
4
6
8
10
12
14
16
18
20
E(MeV)

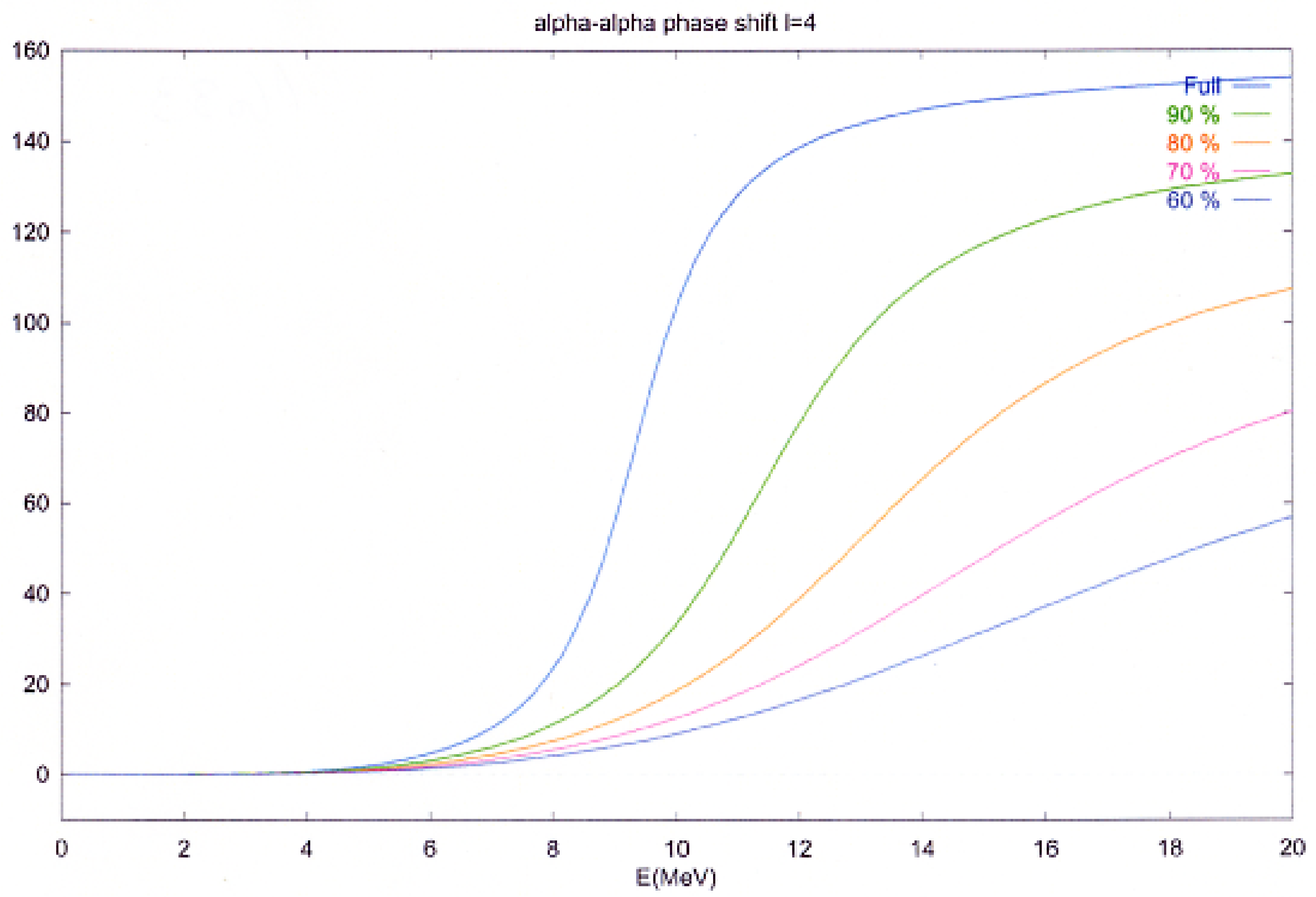
alpha-alpha phase shift l=4
Full
90 %
80 %
70 %
60 %
0
20
40
60
80
100
120
140
160
0
2
4
6
8
10
12
14
16
18
20
E(MeV)

Contour deformation

$$T(E;p,p') = V(p,p') + \int_0^\infty k^2 dk \frac{V(p,k)T(E;k,p')}{E - k^2/2\mu} \quad (1)$$

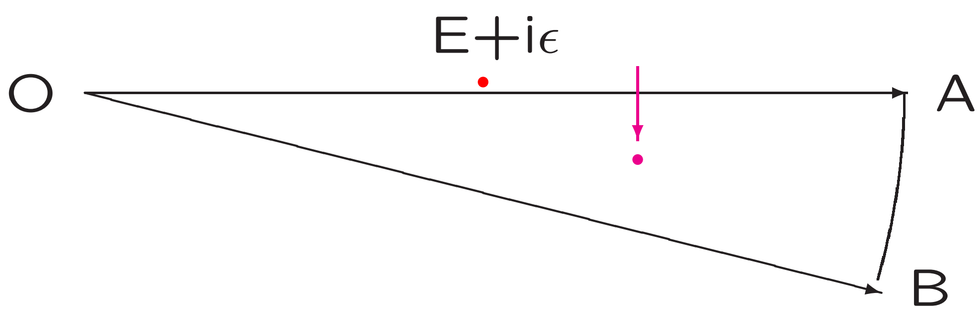

You can replace the contour OA by OB, if

- there are no singularity inside OAB, and
- the contribution from BA is zero.

Contour deformation makes the singularity in the Green's function regular.

At the same time, it makes you to go down on the complex energy plane.

TRACE OF THE TWO-BODY T-MATRIX POLE

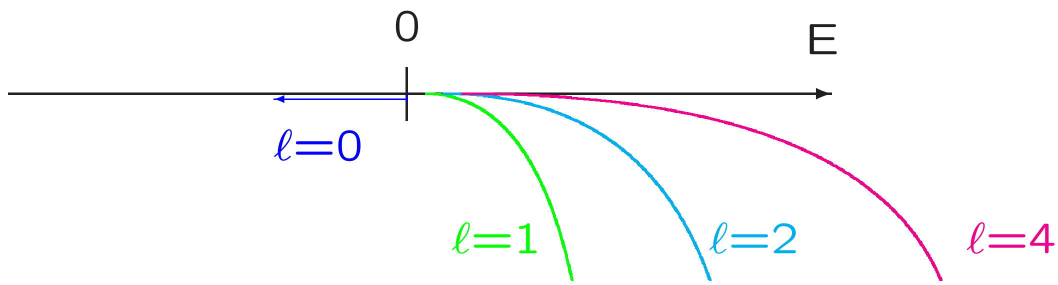

thresholds and cuts in n-d scattering

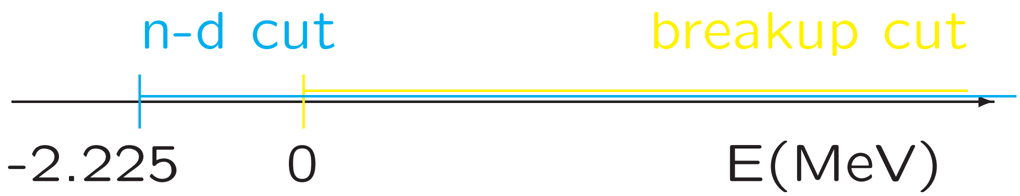

^{6}He

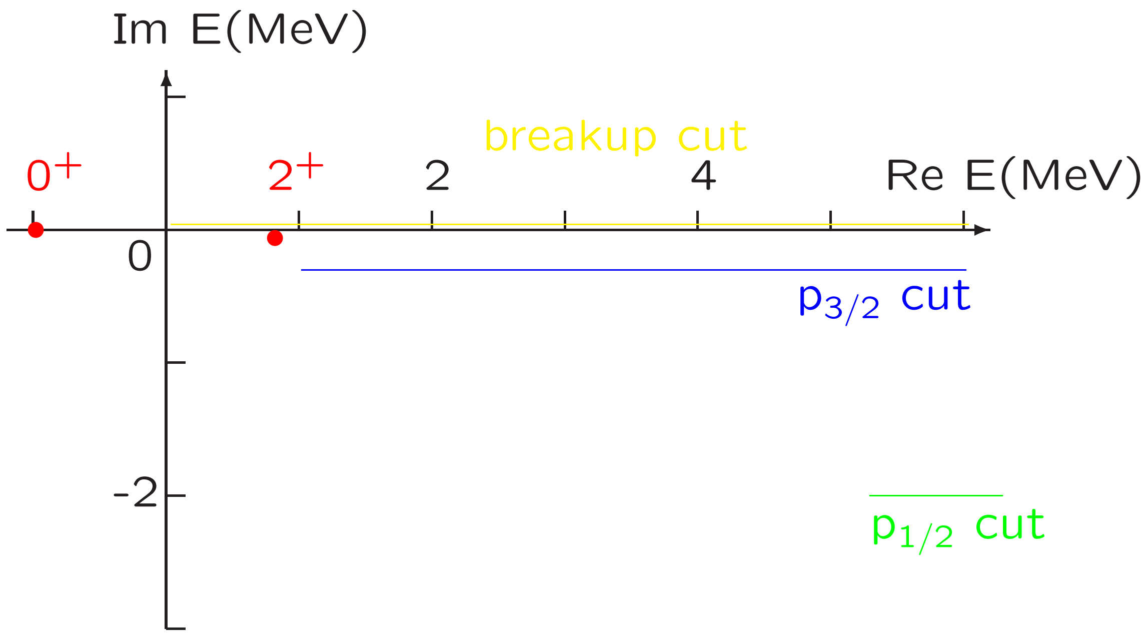

Data taken from experiment.

T=0 states of ^{6}Li

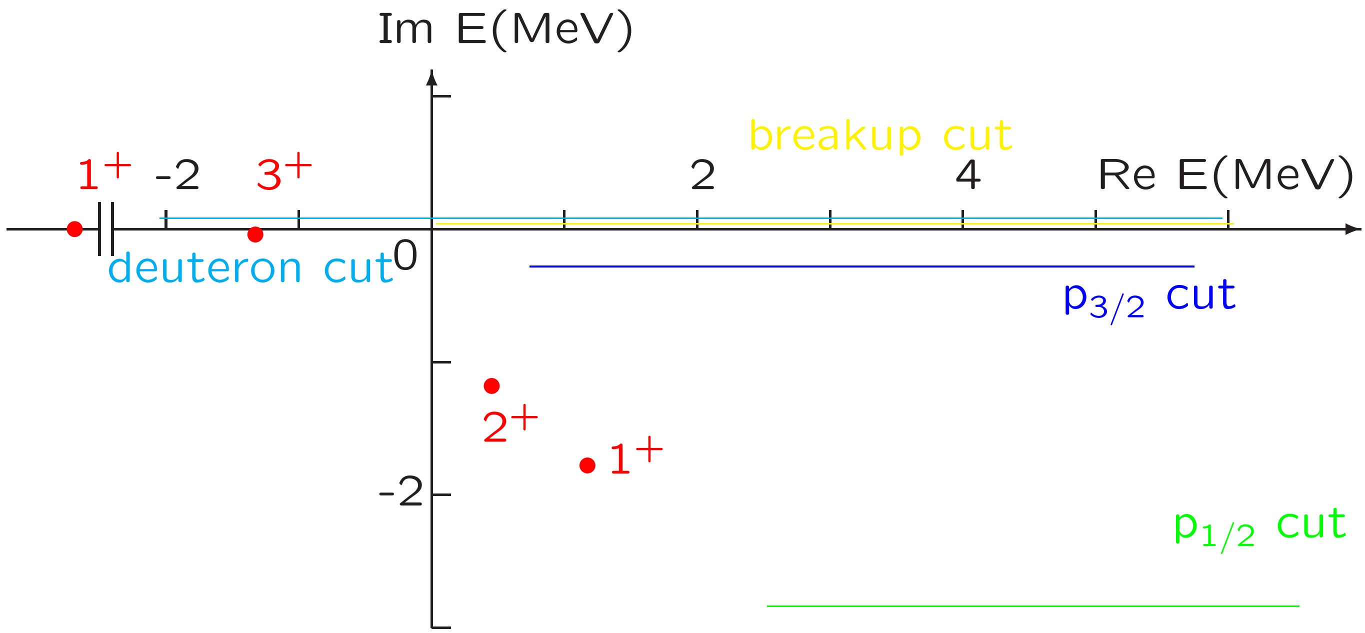

Taken from the calculation by
A. Eskandarian and I.R. Afnan
P.R. C46 (1992) 2344.

2^+ and 1^+ are in different sheet. Reflecting nuclear structure.

There are two critical thresholds:

- Deuteron: Opening d-α channel makes the width of 2^+ and 1^+ very large.

- $p_{3/2}$ in ^{5}He: Positions of these resonances are very close to this threshold. However,
  - In the simple shell model, 1^+ may be described by $(p_{1/2})^2$, while 2^+ by $(p_{3/2},p_{1/2})$.
  - The neutron is "bound" to ^{5}He($p_{3/2}$) in 2^+, and therefore the pole is below the threshold.
  - 1^+ does not have such a structure and therefore the position is above the threshold. However, the FSI in $p_{3/2}$ is very important in the decay mode of 1^+.(Observed in both theory and experiment) So, the position is strongly affected by the threshold.

Level structure of ^{9}Be and $^9_\Lambda$Be

At low energies, they decay into α-α-n(Λ).
Very good example of the three-body resonance.

Many levels are found in experiments. Still spin-parity assignment is difficult for some levels.

important two-body structures:

- α-α rotational band: $\ell = 0$, 2, 4.
- s-wave α-B system
  - Bound state at -3.1 MeV in α-Λ
  - No structure in α-n because of Pauli principle
- p-wave α-B system
  - Strong central and strong ℓ-s force in α-n
  - Poor information but at least not strong central nor ℓ-s force in α-Λ

E. Cravo, A.C. Fonseca, and Y.K.
PRC66, 014001 (2002)

TABLE I. α-α states (MeV) for all three α-α potentials in the absence of Coulomb repulsion.

	UIM	AB	CB
$L=0$	-1.34	-1.33	-1.27
$L=2$	$1.30\text{-}i(0.29)$	$1.36\text{-}i(0.30)$	$1.49\text{-}i(0.44)$
$L=4$	$9.49\text{-}i(1.54)$	$9.58\text{-}i(1.18)$	$10.20\text{-}i(1.87)$

we use, not only Ali-Bodmer (AB) [14] and Chien-Brown (CB) [15] potentials but also one derived in the framework

E. Cravo, A.C. Fonseca, and Y. Koike

PHYSICAL REVIEW C **66**, 014001 (2002)

TABLE IV. $\frac{1}{2}^{+}$ binding energies (MeV) for different α-α and Λ-α interactions. The Coulomb repulsion has been included in all partial waves needed for convergence.

	UIM	AB	CB
TH	−5.96	−5.98	−6.02
MS	−6.50	−6.73	−6.75
DE	−7.08	−7.36	−7.37
DA	−7.74	−8.27	−8.19
Expt. [26]		-6.71	

III. STRUCTURE OF ${}^{9}_{\Lambda}$Be BOUND STATES

TABLE V. Same as in Table **IV** for $\frac{3}{2}^{+}(\frac{5}{2}^{+})$ binding energies (MeV).

	UIM	AB	CB
TH	−3.44	−3.25	−3.17
MS	−4.05	−3.97	−3.80
DE	−4.63	−4.59	−4.41
DA	−5.18	−5.35	−5.05
Expt. [24]		−3.67	

TABLE VI. α-particle rms radius in fermis (point particle) for all α-α and Λ-α potentials.

	$\frac{1}{2}^{+}$			$\frac{3}{2}^{+}(\frac{5}{2}^{+})$		
	UIM	AB	CB	UIM	AB	CB
TH	1.85	1.89	1.87	1.88	1.95	1.95
MS	1.82	1.84	1.82	1.80	1.84	1.83
DE	1.80	1.82	1.80	1.77	1.80	1.80
DA	1.83	1.82	1.81	1.80	1.80	1.81

electric quadrupole moment, and magnetic dipole and octopole moments. Although most of these observables have not been measured for ${}^{9}_{\Lambda}$Be, they provide a better understanding

TABLE VII. Same as in Table **VI** for the Λ-particle rms radius in fermis (point particle).

	$\frac{1}{2}^{+}$			$\frac{3}{2}^{+}(\frac{5}{2}^{+})$		
	UIM	AB	CB	UIM	AB	CB
TH	2.14	2.21	2.18	2.16	2.24	2.22
MS	2.16	2.18	2.15	2.13	2.16	2.16
DE	2.12	2.14	2.11	2.09	2.11	2.11
DA	2.17	2.14	2.14	2.16	2.14	2.15

E. Cravo, A. C. Fonseca and Y. Koike

PHYSICAL REVIEW C **66**, 014001 (2002)

TABLE XI. Same as in Table X for the magnetic octopole moment μ_3 (μ_N fm^2) of the $\frac{3}{2}^+$ and $\frac{5}{2}^+$ excited states.

	$\frac{3}{2}^+$			$\frac{5}{2}^+$		
	UIM	AB	CB	UIM	AB	CB
TH	−0.39	−0.43	−0.43	0.17	0.23	0.23
MS	−0.34	−0.35	−0.35	−0.07	−0.06	−0.05
DE	−0.32	−0.33	−0.33	−0.14	−0.13	−0.13
DA	−0.31	−0.31	−0.31	−0.37	−0.39	−0.38
^{9}Be		6.01	(2.01)			

for the excited state.

In the present work we find two pairs of resonances: one below breakup threshold and one above breakup threshold.

TABLE XII. Position and width of the $\frac{1}{2}^-(\frac{3}{2}^-)$ resonance (MeV) for different α-α and Λ-α potentials in the absence of the Coulomb repulsion.

	UIM		AB		CB	
	E	$\Gamma/2$	E	$\Gamma/2$	E	$\Gamma/2$
TH	−2.00	0.62	−1.98	0.59	−2.03	0.68
MS	−1.69	0.56	−1.65	0.55	−1.67	0.64
DE	−1.89	0.58	−1.84	0.57	−1.86	0.66
DA	−1.92	0.41	−1.89	0.40	−1.87	0.47

TABLE XIII. Position and width of the $\frac{7}{2}^+(\frac{9}{2}^+)$ resonance (MeV) for different α-α and Λ-α potentials in the absence of the Coulomb repulsion.

	UIM		AB		CB	
	E	$\Gamma/2$	E	$\Gamma/2$	E	$\Gamma/2$
TH	1.29	0.14	0.59	0.06	1.66	0.20
MS	0.51	0.06	0.06	0.03	1.09	0.12
DE	−0.06	0.04	−0.51	0.02	0.51	0.09
DA	−0.30	0.04	−0.64	0.02	0.29	0.09

The first one is $\frac{1}{2}^-(\frac{3}{2}^-)$ while the second one is $\frac{7}{2}^+(\frac{9}{2}^+)$.

So far the most accepted understanding of the level structure of $^{9}_{\Lambda}$Be is the work of Yamada *et al.* [30], where a variational $(\alpha+3N+N)$ + Λ cluster model that includes

TABLE XIV. $\frac{1}{2}^-(\frac{3}{2}^-)$ and $\frac{7}{2}^+(\frac{9}{2}^+)$ excitation energies (MeV) for different Λ-α and α-α potentials.

	$\frac{1}{2}^-(\frac{3}{2}^-)$			$\frac{7}{2}^+(\frac{9}{2}^+)$		
	UIM	AB	CB	UIM	AB	CB
TH	6.57	5.74	5.79	9.86	8.31	9.48
MS	7.38	6.84	6.90	9.58	8.55	9.66
DE	7.77	7.30	7.35	9.60	8.63	9.72
DA	8.26	8.15	8.13	9.88	9.40	10.29

Table 9.2: Energy Levels of ^{9}Be

E_x [a] (MeV ± keV)	J^{π}; T	$\Gamma_{c.m.}$ (keV)	Decay	Reactions
g.s.	$\frac{3}{2}^-$; $\frac{1}{2}$		stable	2, 3, 4, 9, 10, 11, 12, 13, 14, 15, 16, 17, 18, 19, 20, 21, 22, 23, 24, 25, 26, 27, 28, 29, 30, 31, 32, 33, 34, 35, 36, 37, 38, 40, 41, 42, 43, 44, 45, 46, 48
1.684 ± 7	$\frac{1}{2}^+$	217 ± 10	γ, n	4, 9, 10, 13, 16, 18, 19, 21, 23, 24, 32, 36, 38, 40
2.4294 ± 1.3	$\frac{5}{2}^-$	0.77 ± 0.15	γ, n, α	4, 9, 10, 11, 12, 16, 17, 18, 19, 21, 22, 23, 24, 25, 26, 32, 33, 35, 36, 37, 38, 40, 44
2.78 ± 120	$\frac{1}{2}^-$	1080 ± 110	n	4, 9, 12, 38, 44
3.049 ± 9	$\frac{5}{2}^+$	282 ± 11	γ, n	4, 9, 16, 18, 19, 21, 23, 24, 32, 36, 38, 40
4.704 ± 25	$(\frac{3}{2})^+$	743 ± 55	γ, n	4, 9, 16, 21, 23, 24, 38, 44
6.76 ± 60	$\frac{7}{2}^-$	1540 ± 200	γ, n	9, 11, 16, 17, 18, 19, 21, 23, 24, 25, 35, 40
7.94 ± 80	$(\frac{1}{2}^-)$	≈ 1000		12, 19
11.283 ± 24		575 ± 50	n	9, 12, 19, 24, 35, 36
11.81 ± 20	$T = \frac{1}{2}$	400 ± 30	γ, n	9, 12, 13, 37, 44
13.79 ± 30	$T = \frac{1}{2}$	590 ± 60	γ, n	9, 16, 37
14.3922 ± 1.8 [c]	$\frac{3}{2}^-$; $\frac{3}{2}$	0.381 ± 0.033	γ, n, α	9, 16, 19, 23, 36, 37
14.4 ± 300		≈ 800		36
15.10 ± 50			γ	16, 37
15.97 ± 30	$T = \frac{1}{2}$	≈ 300	γ	16, 37
16.671 ± 8	$(\frac{5}{2}^+)$	41 ± 4	γ	9, 16, 19, 36
16.9752 ± 0.8 [d]	$\frac{1}{2}^-$; $\frac{3}{2}$	0.49 ± 0.05	γ, n, p, d	4, 5, 6, 15, 16
17.298 ± 7	$(\frac{5}{2})^-$	200	γ, n, p, d, α	5, 6, 7, 13, 16, 19
17.493 ± 7	$(\frac{7}{2})^+$	47	γ, n, p, d, α	5, 6, 7, 16, 19
18.02 ± 50			γ	16
18.58 ± 40			γ, n, p, d, α	6, 16

Table-1

Experimentally well established low lying levels

	Present (Koike)		Arai *et al.*		SC and NM	
	E (MeV)	Γ (MeV)	E (MeV)	Γ (MeV)	E (MeV)	Γ (MeV)
$3/2^-$	0	0	0	0	0	0
$1/2^+$	(virtual state)				1.684	0.217
$5/2^-$	2.33	$< 10^{-3}$	2.27	0.001	2.429	0.00077
$1/2^-$	2.82	0.50	2.63	0.46	2.780	1.08
$5/2^+$	3.91	0.35	3.41	0.6	3.049	0.282
$3/2^+$	4.95	1.95	4.7	1.6	4.704	0.743

Theory ← | → Experiment

Table-2

Higher lying resonances

Energy	Present (Koike)			Arai *et al.*			SC			NM		
(MeV)	E	Γ	J^π	E	Γ	J^π	E	Γ	J^π	E	Γ	J^π
< 6.7	tail of the $\frac{7}{2}^+$			4.3	0.8	$\frac{3}{2}^-$	None			5.59	1.33	$\frac{3}{2}^-$
~ 6.7	6.68	1.98	$\frac{7}{2}^-$	6.46	1.2	$\frac{7}{2}^-$	6.76	1.54	$\frac{7}{2}^-$	6.38	1.21	$\frac{7}{2}^-$
~ 6.7	6.65	2.46	$\frac{9}{2}^+$	6.3	2.9	$\frac{9}{2}^+$	None			6.76	1.33	$\frac{9}{2}^+$
> 6.7	8.13	6.32	$\frac{7}{2}^+$	7.9	2.1	$\frac{5}{2}^-$	7.94	~ 1	$\frac{1}{2}^-$	None		
11.28	10.36	1.14	$\frac{9}{2}^-$	None			11.28	0.575		11.28	1.14	$\frac{7}{2}^+$

Theory ← | → Experiment